Numerical simulation of crack growth and coalescence in rock-like materials by using General Particle Dynamics

Xiao-Ping Zhou

School of Civil Engineering, Chongqing University

Dec, 2016

Outline

- *Brief Description of General Particle Dynamics*
- *Growth and Coalescence of Flaws Subjected to Static Compression*
- *Kinetic Effect on Friction in the Fracture Process of Rocks*
- *Fracture in Rock-Like Materials Subjected to Impact Loads*
- *Discussions and Conclusions*

Traditional Numerical Methods

- There are some traditional numerical simulation methods: FEM, MD, SPH etc.

Shortcomings of Traditional Numerical Methods

- The traditional methods are based on classical local theory, which is acceptable in the macroscale . The validity of locality is questionable in the field of microscale mechanics, mesoscale mechanics and some multiscale mechanics problem

General Particle Dynamics Theory

- **It is based on a nonlocal theory of continuous media which establishes the connection between classical continuum mechanics and molecular dynamics. So it is validating in simulating some multi-scale problem.**

- **With the GPD theory, damage in the material is simulated in a much more realistic manner compared to the classical continuum-based methods.**

Brief Description of General Particle Dynamics

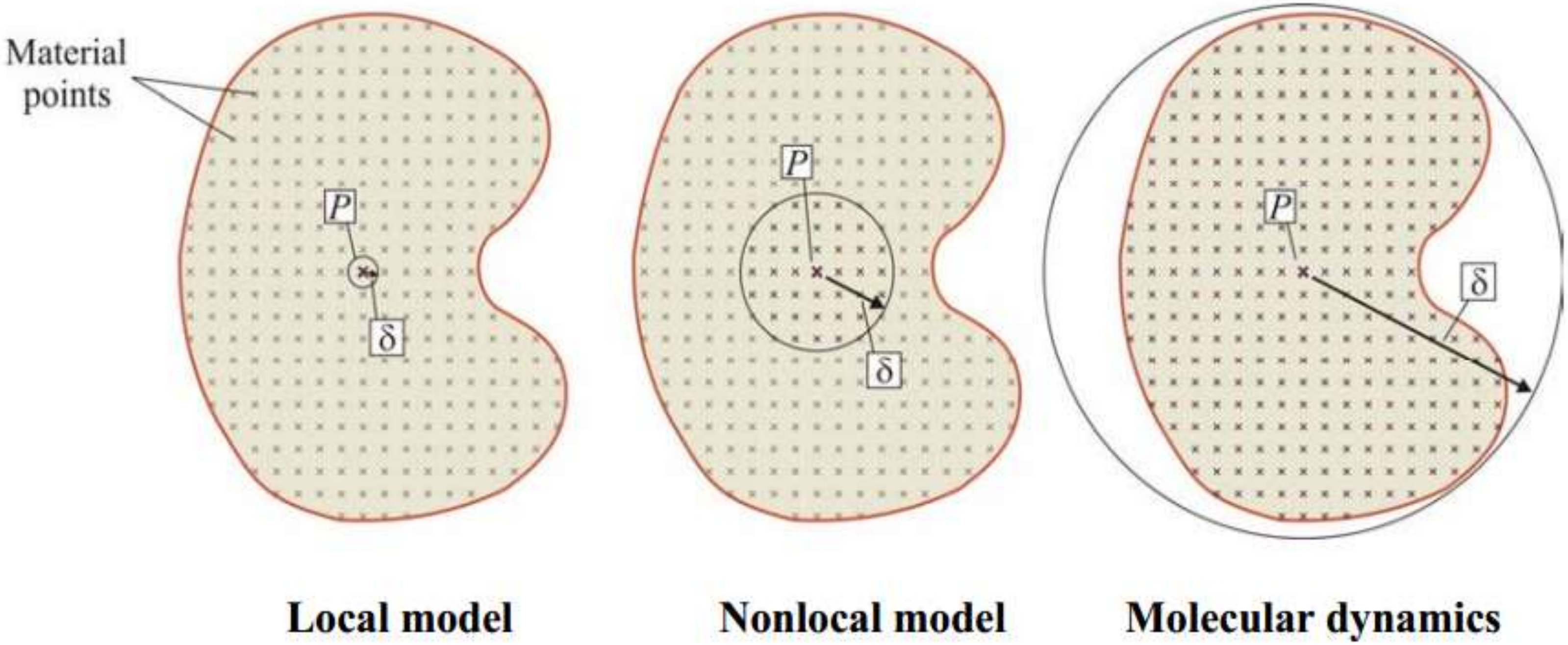

Fig. 1 Relationship among length scales

Brief Description of General Particle Dynamics

Stresses in the virtual-bonds

General Particle Dynamics is bond-based meshfree method. The axial tensile stress is calculated on center orthogonal to R-axis and directed along $\overrightarrow{r_j - r_i}$, shear stress is calculated on direction S, which is normal to R-axis in the local R-S coordinate system

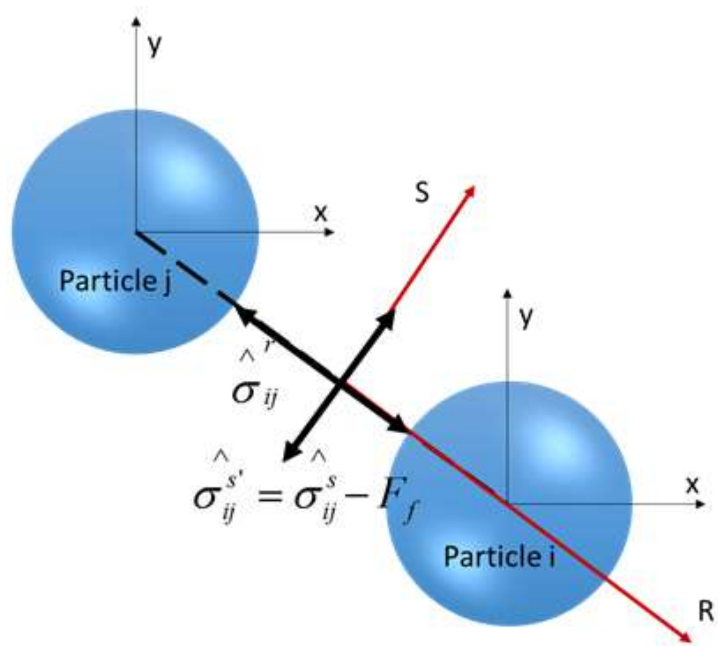

Fig. 2 Tensile stress and shear stress on the virtual-bond between contacting particles

The normal stress is expressed as

$$\hat{\sigma}_{ij}^{r} = \frac{\sigma_i^r \rho_j C_j^l + \sigma_j^r \rho_i C_i^l + \rho_i C_i^l \rho_j C_j^l (u_j^r - u_i^r)}{\rho_i C_i^l + \rho_j C_j^l} \qquad (1)$$

where,

$$u_{ij}^{r} = \vec{T}^{r} \vec{u}_{ij} = \frac{(x_{ij} u_{ij}^{x} + y_{ij} u_{ij}^{y})}{\left| r_j - r_i \right|} \qquad (2)$$

When the friction is not considered, the shear stress is expressed as

$$\hat{\sigma}_{ij}^{s} = \frac{\sigma_i^s \rho_j C_j^t + \sigma_j^s \rho_i C_i^t + \rho_i C_i^t \rho_j C_j^t (u_j^s - u_i^s)}{\rho_i C_i^t + \rho_j C_j^t} \quad \textbf{(3)}$$

where,

$$u_{ij}^{s} = \vec{T}^{s} \vec{u}_{ij} = \frac{(y_{ij} u_{ij}^{x} + x_{ij} u_{ij}^{y})}{\left| r_j - r_i \right|} \quad \textbf{(4)}$$

When the friction is considered, the effective shear stress is obtained as

$$\hat{\sigma}_{ij}^{s'} = \hat{\sigma}_{ij}^{s} + \hat{\sigma}_{ij}^{r} \mu \qquad (when \quad \hat{\sigma}_{ij}^{r} \le 0) \quad \textbf{(5)}$$

where, μ is the frictional coefficient of the parent material.

Damage in particles

The non-linear Unified Strength criterion is applied to determine the damage in particles.

$$F = [\sigma_1 - \frac{1}{1+b}(b\sigma_2 + \sigma_3)]^2 - \frac{m\sigma_c}{1+b} \times (b\sigma_2 + \sigma_3) - s\sigma_c^2 = 0 \qquad when\ F \geq F' \tag{6}$$

$$F' = [\frac{1}{1+b}(b\sigma_2 + \sigma_1) - \sigma_3]^2 - m\sigma_c\sigma_3 - s\sigma_c^2 = 0 \qquad when\ F' > F \tag{7}$$

Damage in particles

Now we introduce a parameter f, coined as the 'interaction factor' which defines the level of interaction between the i-th and the j-th particles.

$$D = 0, and \quad f = 1, \quad (if \;\; \sigma_i < \sigma_{\max}) \qquad \textbf{(8)}$$

$$D = 1, and \quad f = 0, \quad (if \;\; particle\ damaged) \qquad \textbf{(9)}$$

where D is the Damage factor, and f is the interaction factor.

Damage in particles

In order to model the damage growth, a linear elastic brittle law is used

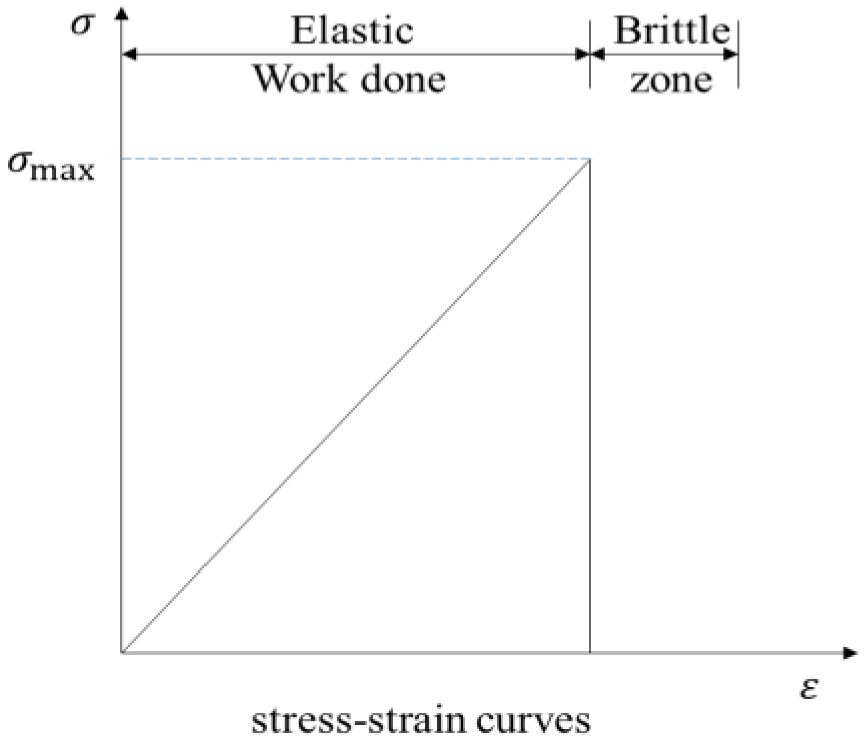

Fig. 3. linear elastic brittle law

Damage in particles

The discrete conservation equations of General Particle Dynamics (GPD) are expressed as

$$\frac{d\rho_i}{dt} = \sum_{j\in U} m_j v_{ij}^{\beta} W_{ij,\beta} + f \cdot \sum_{j\in D} m_j v_{ij}^{\beta} W_{ij,\beta} \tag{10}$$

$$\frac{dv_i^{\alpha}}{dt} = -\sum_{j\in U} m_j \left(\frac{\sigma_i^{\alpha\beta}}{\rho_i^2} + \frac{\sigma_j^{\alpha\beta}}{\rho_j^2} + \Pi_{ij}\right) W_{ij,\beta} - f \cdot \sum_{j\in D} m_j \left(\frac{\sigma_i^{\alpha\beta}}{\rho_i^2} + \frac{\sigma_j^{\alpha\beta}}{\rho_j^2} + \Pi_{ij}\right) W_{ij,\beta} \tag{11}$$

$$\frac{de_i}{dt} = \frac{1}{2} \sum_{j\in U} m_j v_{ij}^{\alpha} \left(\frac{\sigma_i^{\alpha\beta}}{\rho_i^2} + \frac{\sigma_j^{\alpha\beta}}{\rho_j^2} + \Pi_{ij}\right) W_{ij,\beta} + \frac{f}{2} \cdot \sum_{j\in D} m_j v_{ij}^{\alpha} \left(\frac{\sigma_i^{\alpha\beta}}{\rho_i^2} + \frac{\sigma_j^{\alpha\beta}}{\rho_j^2} + \Pi_{ij}\right) W_{ij,\beta} \tag{12}$$

where, U denotes undamaged particles, D denotes Damaged particles

Damage in the virtual-bonds

The sequence of failure of such neighboring bonds are captured to trace the propagation of cracks

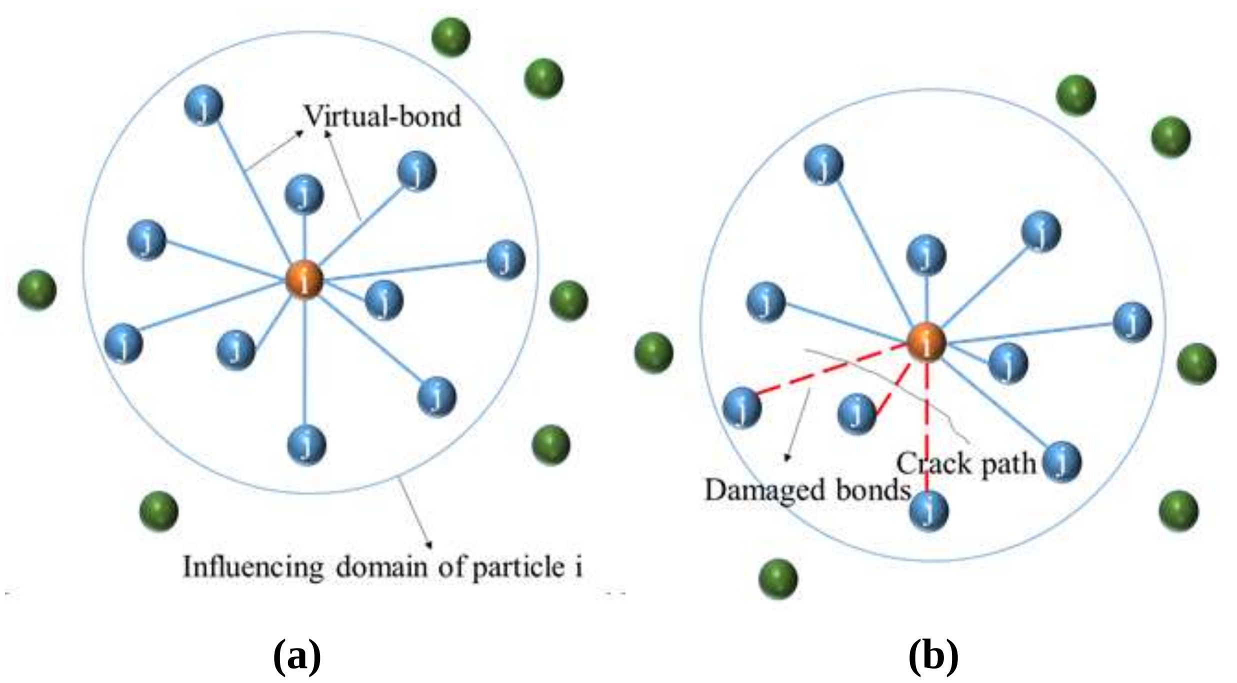

Fig.4 Virtual-bonds among neighboring particles: (a)undamaged bonds; (b)damaged bonds

Particle distribution in the numerical models

In GPD method, the statistical distribution of the elemental mechanical parameters is described by the Weibull distribution function.

$$W(x) = \frac{\omega}{x_0}\left(\frac{x}{x_0}\right)^{\omega-1}\exp\left[-\left(\frac{x}{x_0}\right)^{\omega}\right] \qquad \textbf{(13)}$$

where, ω defines the shape of the Weibull distribution function, and it can be referred to as the homogeneity index, x is the mechanical parameter of one particle, and x_0 is the even value of the parameter of all the particles.

Weibull’s distribution

For cracking problem, only the uniaxial compressive strength σ_c of particles is described by using the Weibull’s distribution.

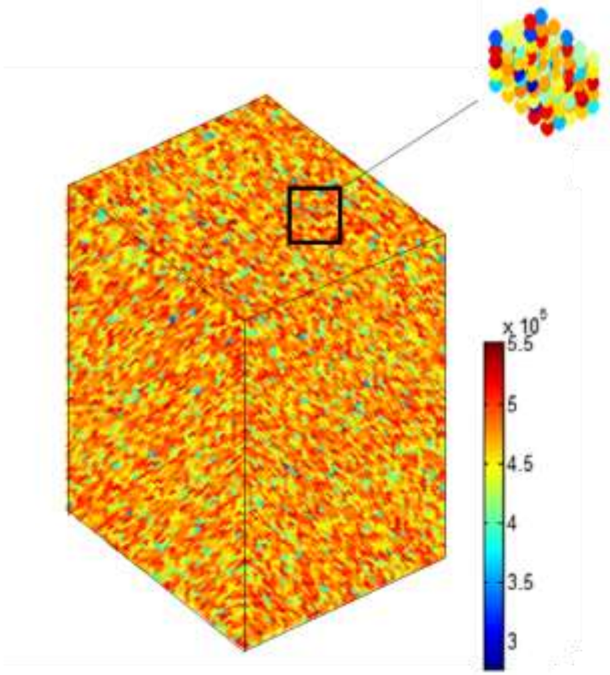

Fig. 5 The uniaxial strength distribution of particles in the numerical model (Pa)

Bi, J., Zhou, X., and Xu, X. (2016). "Numerical Simulation of Failure Process of Rock-Like Materials Subjected to Impact Loads." *Int. J. Geomech.* , 10.1061/(ASCE)GM.1943-5622.0000769 , 04016073.

Outline

- ***Brief Description of General Particle Dynamics***
- ***Growth and Coalescence of Flaws Subjected to Static Compression***
- ***Friction Effect on the Fracture Process of Rocks***
- ***Fracture in Rock-Like Materials Subjected to Impact Loads***
- ***Discussions and Conclusions***

Compared with the previous experimental results

It is found that numerical result of crack propagation paths is in good agreement with the experimental result.

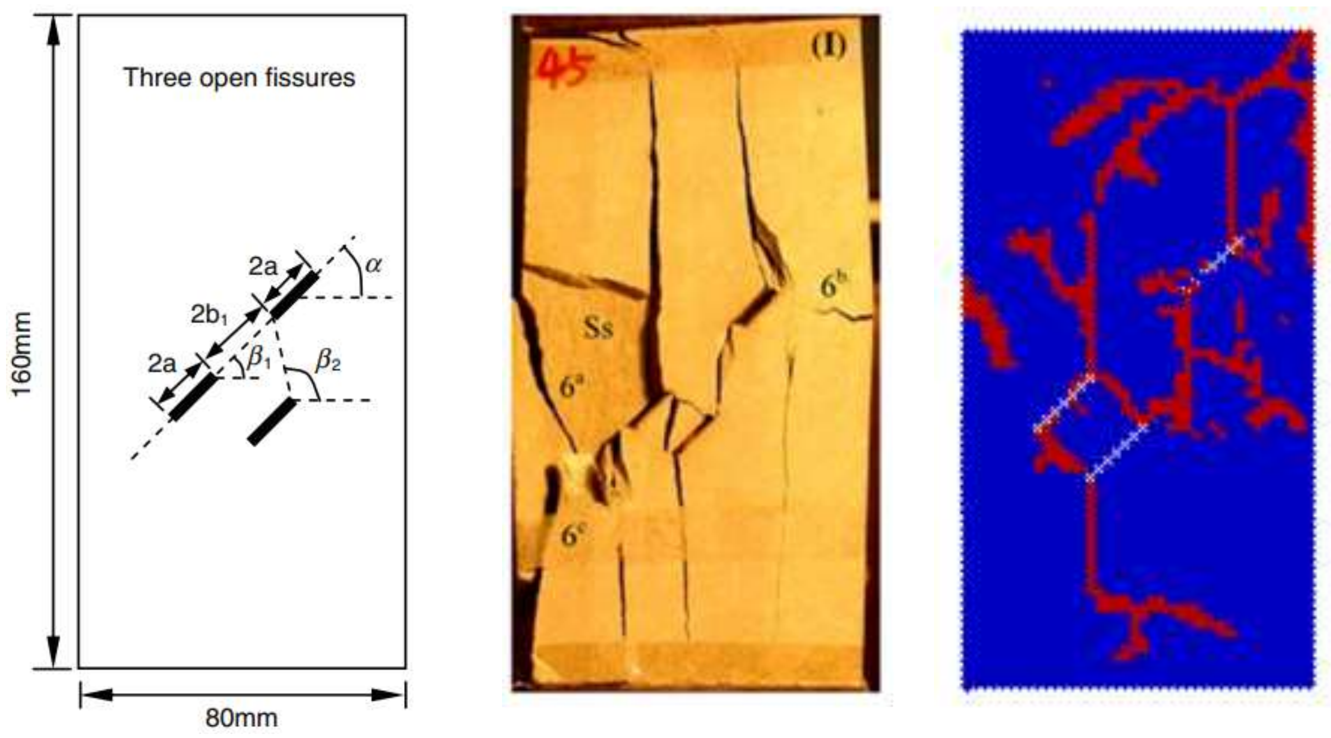

(a) (b) (c)

Fig. 6 (a) Geometry of the three flaws in the sandstone specimens. (b) experimental results on crack coalescence process of a sandstone specimen containing three flaws under uniaxial compression, (c) the numerical result of crack propagation paths.

Geometries of the 2D numerical model

The coefficient of the modeling material are γm=16KN/m3,σc0=0.483MPa, μ=0.754, respectively. Young's modulus is 1.6MPa and Poisson ratio is 0.32. The flaw angles are equal to 45^0 .

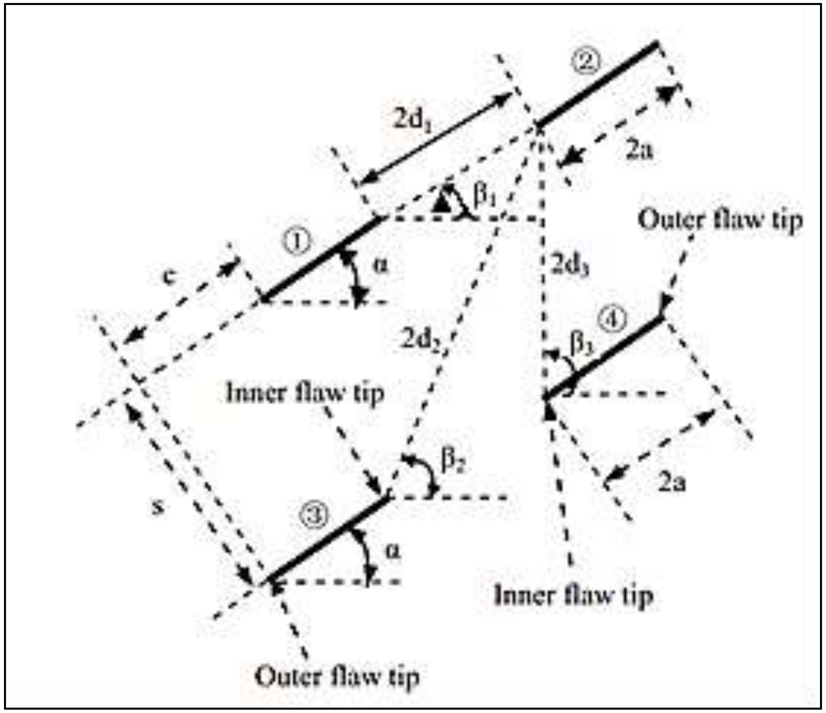

Fig. 7 The layout of samples containing four flaws with different non-overlapping length c=0mm; c=10mm;c=20mm.

Numerical results of 2D models under uniaxial compression

In Fig. 8(a), the out-of-plane shear crack coalesces with the quasi-coplanar secondary cracks; in Fig. 8(b), The quasi-coplanar secondary crack coalesces with each other; in Fig. 8(c), the out-of-plane shear crack coalesces with the quasi-coplanar secondary crack.

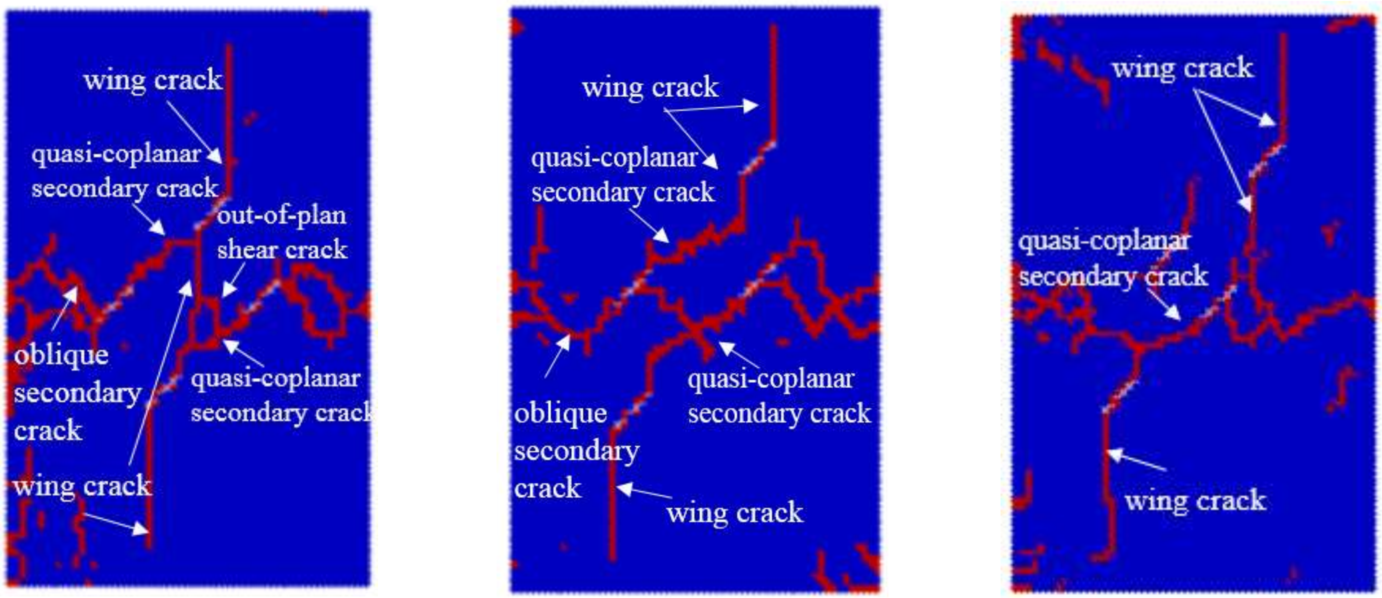

(a) (b) (c)

Fig. 8 The numerical simulation of crack coalescence of rock-like samples under uniaxial compressive loads: (a) c=0mm;(b) c=10mm;(c)c=20mm.

Geometries of the 3D numerical model under uniaxial compression

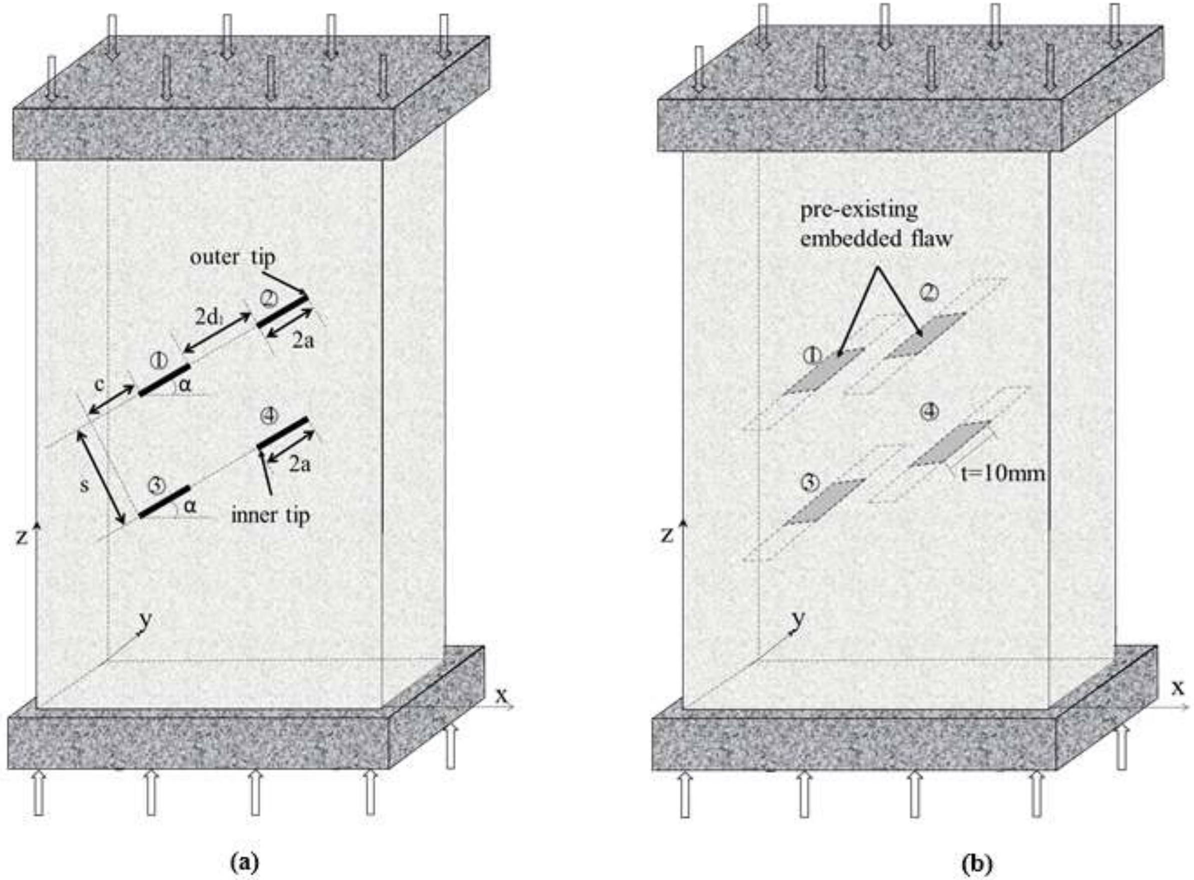

Fig. 9 (a) the samples containing four penetrating flaws; (b) the samples containing four embedded flaws.

Numerical results of 3D models containing four pre-existing penetrating flaws under uniaxial compression

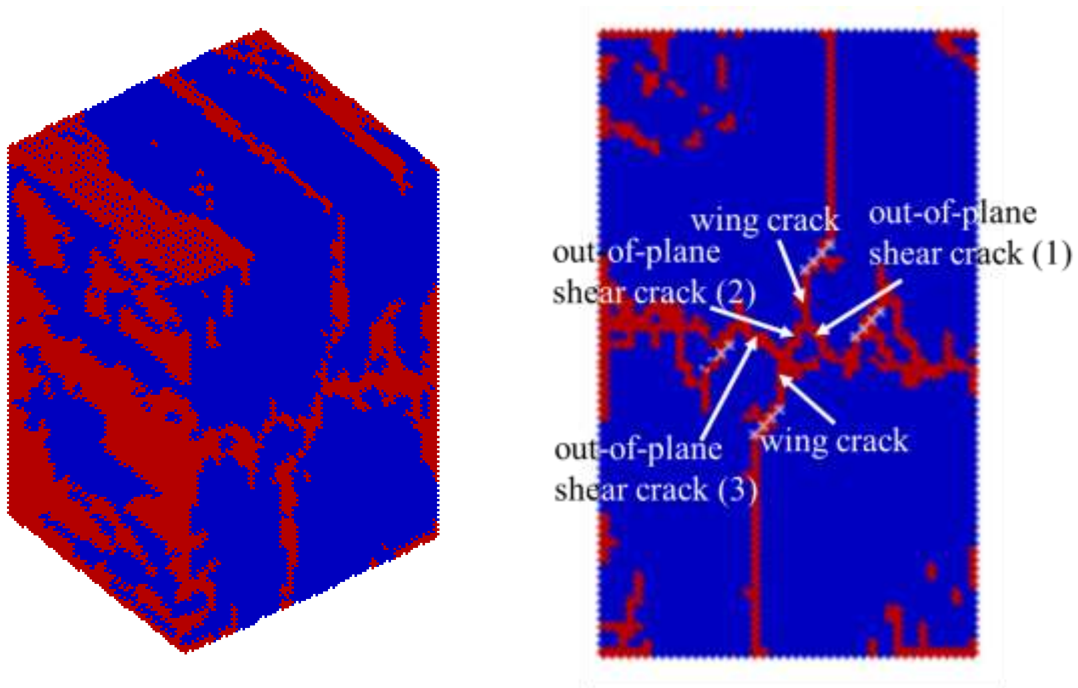

(a) (b)

Fig. 10 The sample containing four pre-existing penetrating flaws with non-overlapping length c=0mm :(a) 3D drawn of crack propagation paths, (b) the cross section of crack propagation paths.

The out-of-plane shear crack coalesces with the wing cracks

Numerical results of 3D models containing four pre-existing penetrating flaws under uniaxial compression

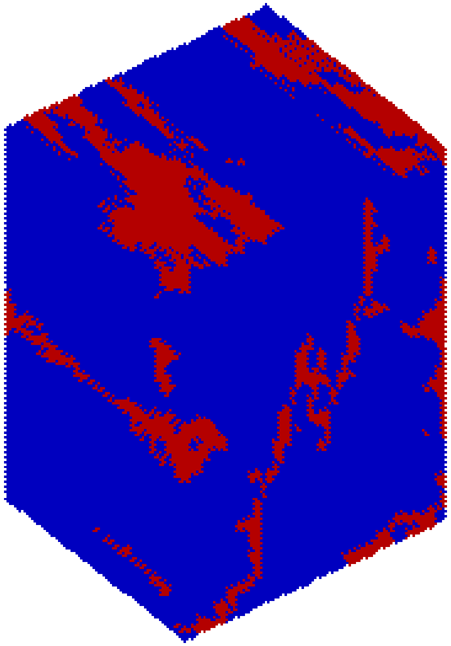

(a)

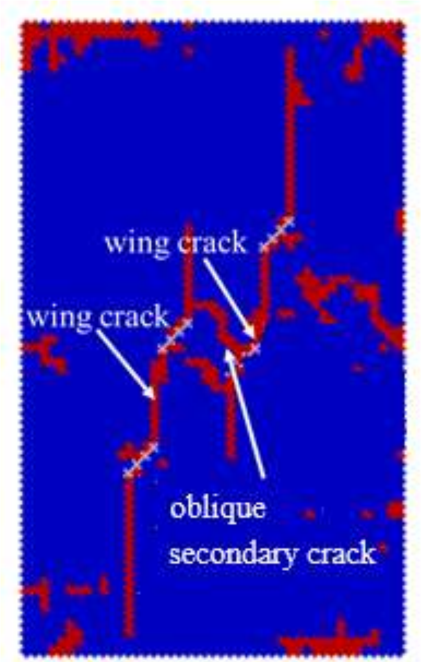

(b)

Fig. 12 The sample containing four pre-existing penetrating flaws with non-overlapping length c=20mm :(a) 3D drawn of crack propagation paths, (b) the cross section of crack propagation paths.

The oblique secondary crack coalesces with the wing crack.

Numerical results of 3D models containing four pre-existing embedded flaws under uniaxial compression

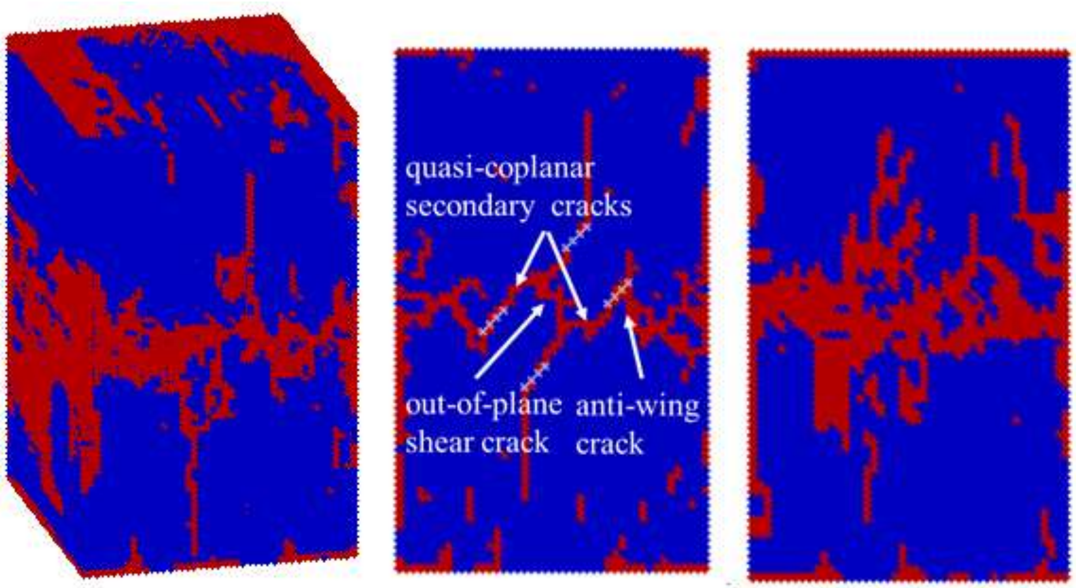

(a) (b) (c)

Coalescence of the out-of-plane shear crack and the wing crack is found in the sample with four pre-existing embedded flaws

Fig. 13 The sample containing four pre-existing embedded flaws with non-overlapping length c=0mm: (a) The front of paths of crack propagation, (b) the cross section of paths of crack propagation, (c) the back of paths of crack propagation .

Numerical results of 3D models containing four pre-existing embedded flaws under uniaxial compression

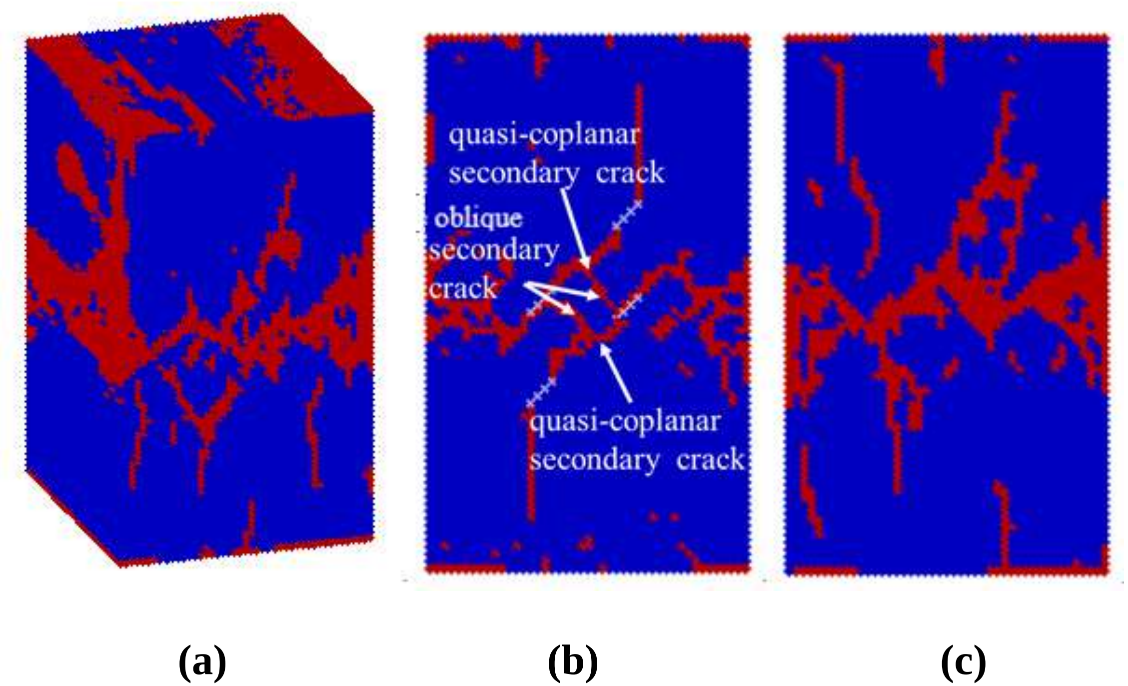

Fig. 14. The sample containing four pre-existing embedded flaws with non-overlapping length c=10mm: (a) The front of paths of crack propagation, (b) the cross section of paths of crack propagation, (c) the back of paths of crack propagation .

Coalescence of the oblique secondary crack and the quasi-coplanar secondary crack are observed in the sample with four pre-existing embedded flaws

Numerical results of 3D models under uniaxial compression

For the samples containing four pre-existing embedded flaws, the peak strength increases when the non-overlapping length increases from 0mm to 10mm, while the peak strength decreases when the non- overlapping length increases from 10mm to 20mm. For the samples containing four pre-existing penetrating flaws, it is opposite.

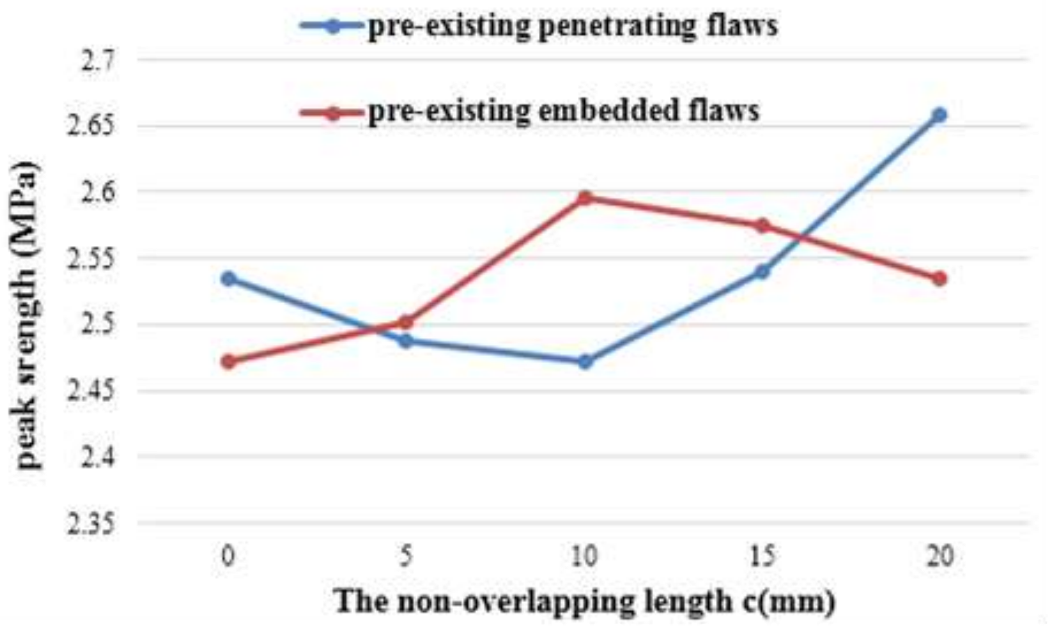

Fig. 16 The peak strength of the samples versus the non-overlapping length

Experimental and Numerical results under biaxial compression

In order to validate GPD3D, the numerical results from GPD3D will be compared with the experimental results

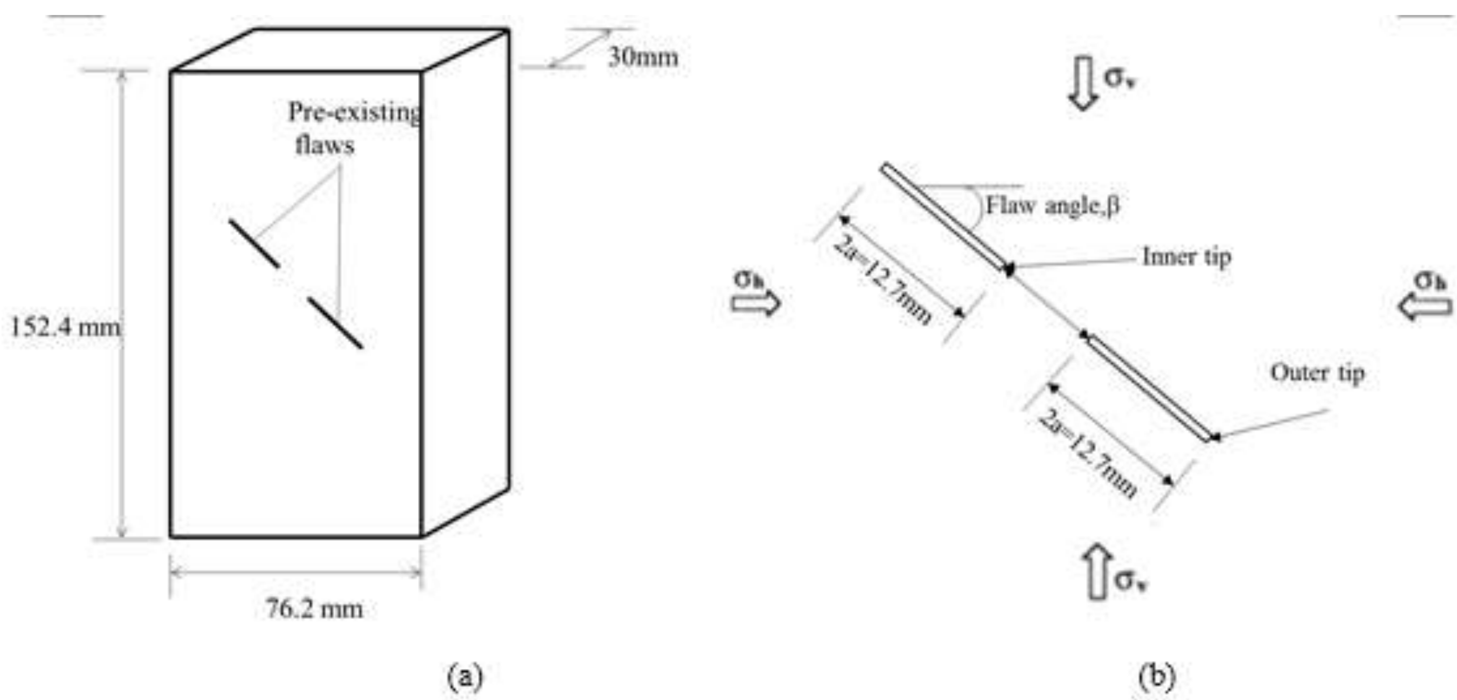

Fig. 17 Geometries of rock specimens containing the two pre-existing collinear penetrating flaws. (a) Overall view. (b)Detail

Experimental and Numerical results under biaxial compression

Numerical result is in good agreement with the experimental result.

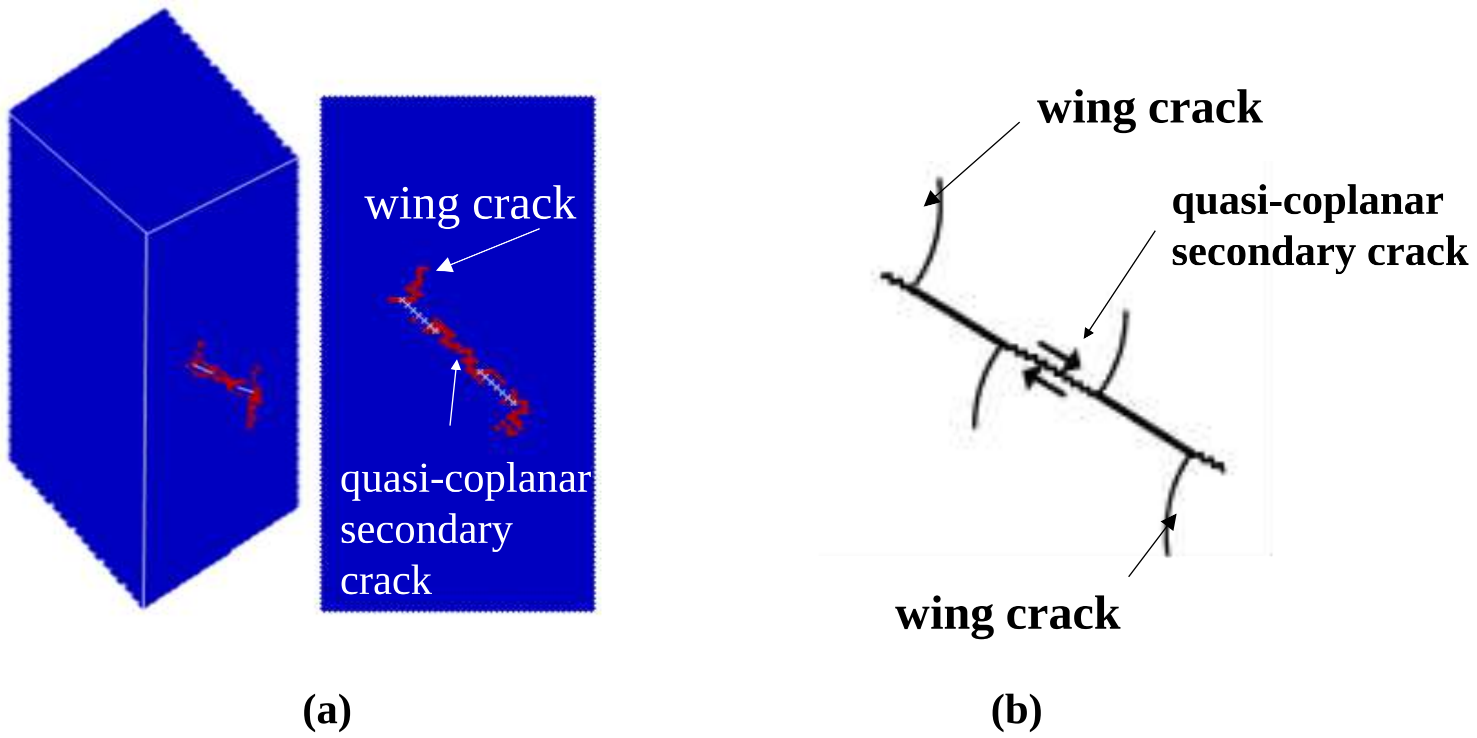

Fig. 18 (a) numerical result;(b) The coalescence patterns of cracks in experimental samples under biaxial compression (Bobet and Einstein, 1998)

Geometries of the 3D numerical model under biaxial compression

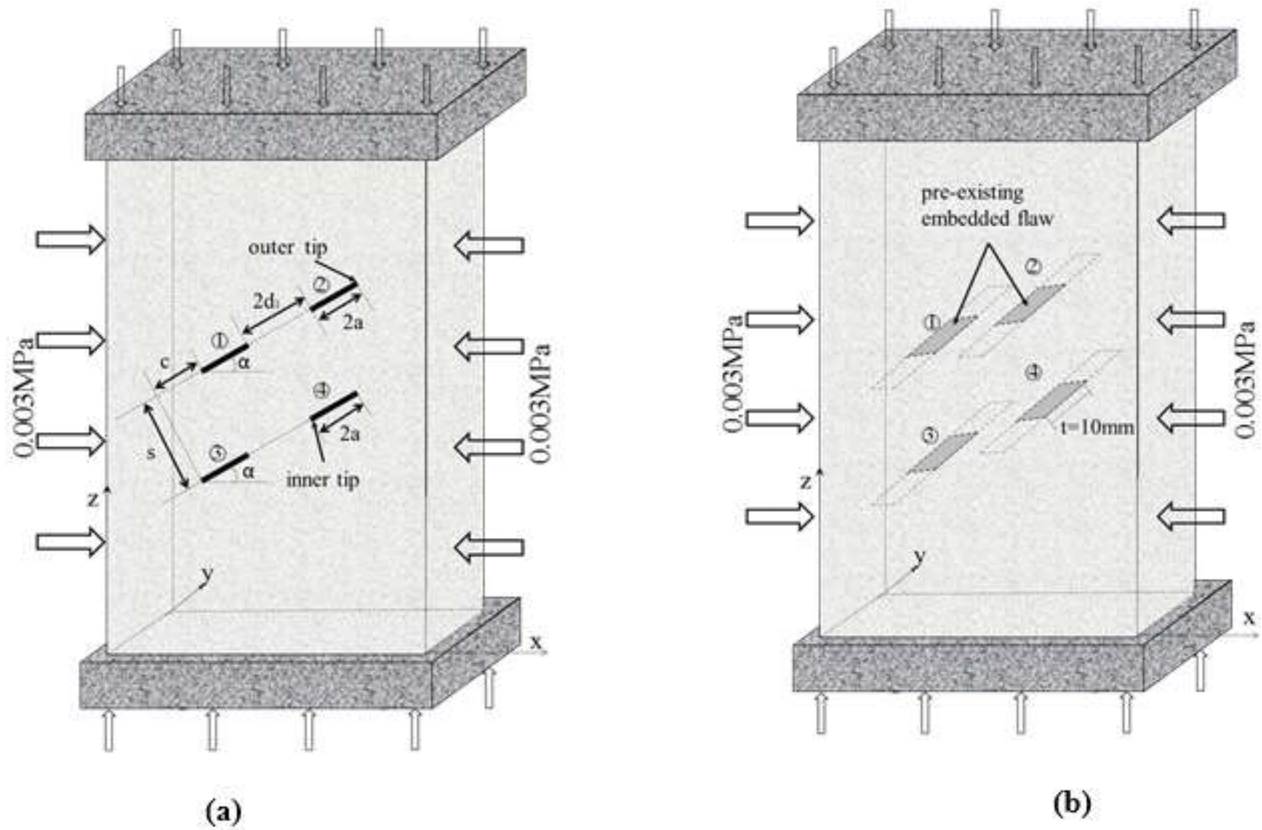

Fig. 19 The layout of samples containing four pre-existing flaws under biaxial compression with the lateral stress of 0.003MPa (a) the pre-existing penetrating flaws (b) the pre-existing embedded flaws

Numerical results of 3D models containing four pre-existing embedded flaws under biaxial compression

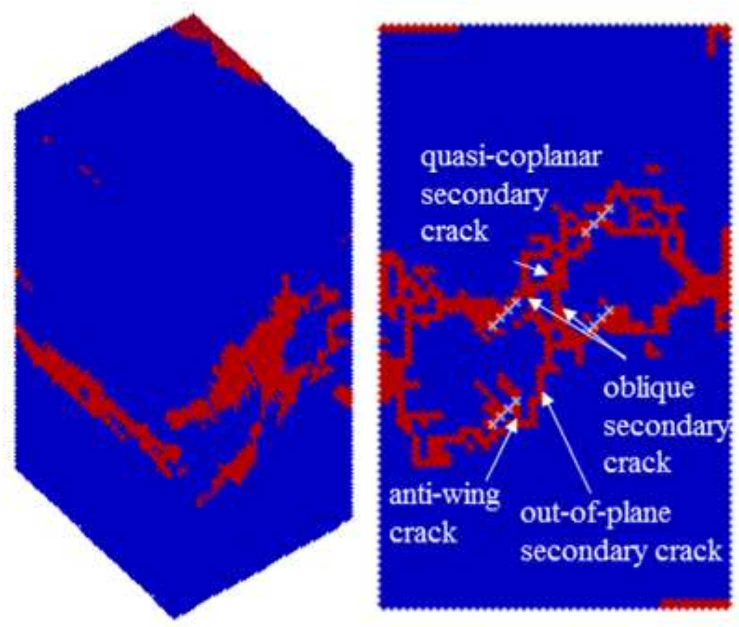

Fig. 24 (a) 3D drawn of propagation paths of the pre-existing flaws;(b) the cross section of propagation paths of the pre-existing flaws with non-overlapping length c=10mm in the sample

The coalescence of the oblique secondary cracks are observed in the sample under biaxial compression

Outline

- *Brief Description of General Particle Dynamics*
- *Growth and Coalescence of Flaws Subjected to Static Compression*
- *Friction Effect on the Fracture Process of Rocks*
- *Fracture in Rock-Like Materials Subjected to Impact Loads*
- *Discussions and Conclusions*

The frictional interaction algorithm

The support domain of the *i*-th particle is composed of two entirely different types of particles, which is located on either side of the pre-existing flaw

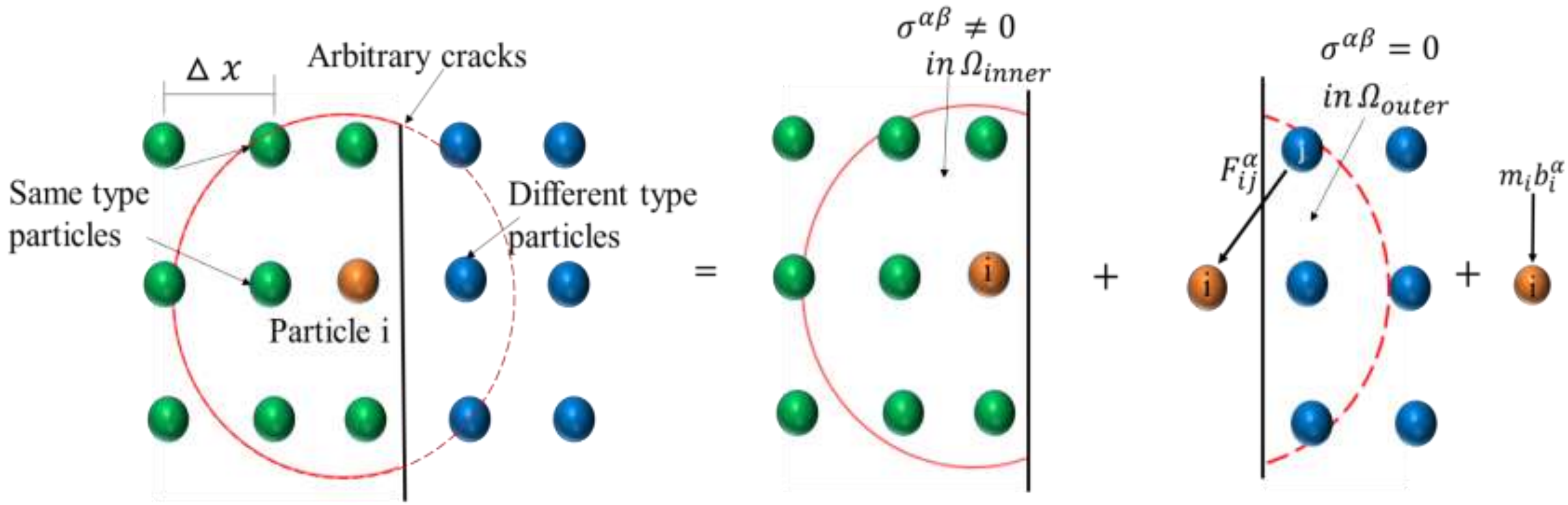

Fig. 26. Decomposition of acceleration for the particle *i*.

If the contact function is considered, the equation of motion for the ith contact particle can finally be written as

$$\frac{dv_i^{\alpha}}{dt} = \sum_{j\in\Omega_{inner}} m_j\left(\frac{\sigma_i^{\alpha\beta}}{\rho_i^2} + \frac{\sigma_j^{\alpha\beta}}{\rho_j^2} + \Pi_{ij}\right)W_{ij,\beta} + \sum_{j\in\Omega_{outer}} \frac{F_{ij}^{\alpha}}{m_i} + b^{\alpha} \qquad \textbf{(14)}$$

The discrete conservation equations of contact problem for General Particle Dynamics are expressed as

$$\frac{d\rho_i}{dt} = \sum_{j\in U} m_j v_{ij}^{\beta} W_{ij,\beta} + f \cdot \sum_{j\in D_m} m_j v_{ij}^{\beta} W_{ij,\beta} \quad \textbf{(15a)}$$

$$\frac{dv_i^{\alpha}}{dt} = \sum_{j\in U} m_j \left(\frac{\sigma_i^{\alpha\beta}}{\rho_i^2} + \frac{\sigma_j^{\alpha\beta}}{\rho_j^2} + \Pi_{ij}\right) W_{ij,\beta} + f \cdot \sum_{j\in D_m} m_j \left(\frac{\sigma_i^{\alpha\beta}}{\rho_i^2} + \frac{\sigma_j^{\alpha\beta}}{\rho_j^2} + \Pi_{ij}\right) W_{ij,\beta} + \sum_{j\in D_m} \frac{F_{ij}^{\alpha}}{m_i} \quad \textbf{(15b)}$$

The initiation and propagation of cracks considering the frictional effects in the sample containing a pre-existing flaw under uniaxial compression

Calculation Parameters	
ρ=2650 kg/m^3	m=3.5 (Hoek-Brown strength criterion)
E=80 MPa	s=0.8 (Hoek-Brown strength criterion)
v=0.25	$\triangle$t=1 μs (time step of GPD)
σ_c = 0.8MPa	uniaxial compressive strength
$\omega = 10$	homogeneous index

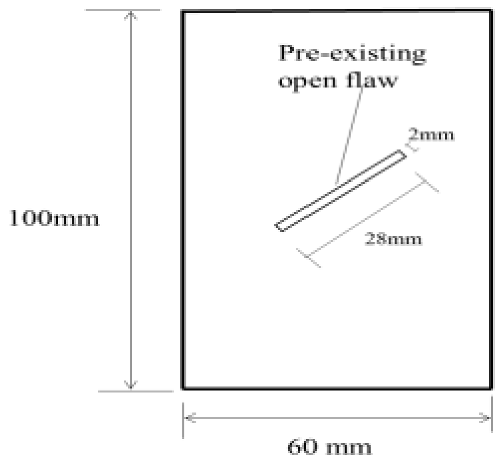

(a) The sample containing the open flaw

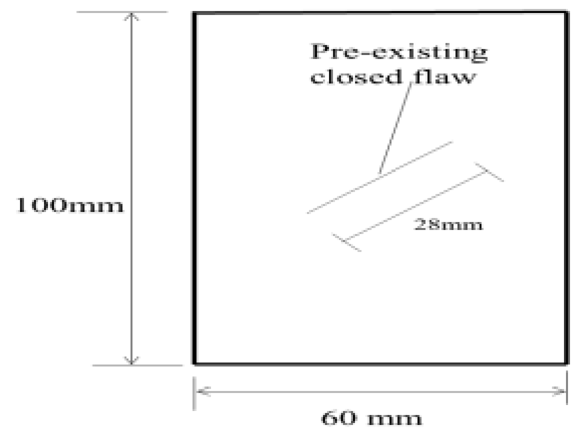

(b) The sample containing the closed flaw

Fig.27 The geometric model

Numerical results

The first sample containing an open flaw as the sample 1, the second sample containing a closed flaw without the frictional effects as the sample 2, and the third sample containing a closed flaw with the frictional effects($\mu_k = 0.2$ **and** $\mu_s = 0.7$**) as the sample 3. Initiation angle of the wing cracks in sample 1 is equal to 90^0, initiation angle of the wing cracks in sample 2 and 3 is more than 90^0.**

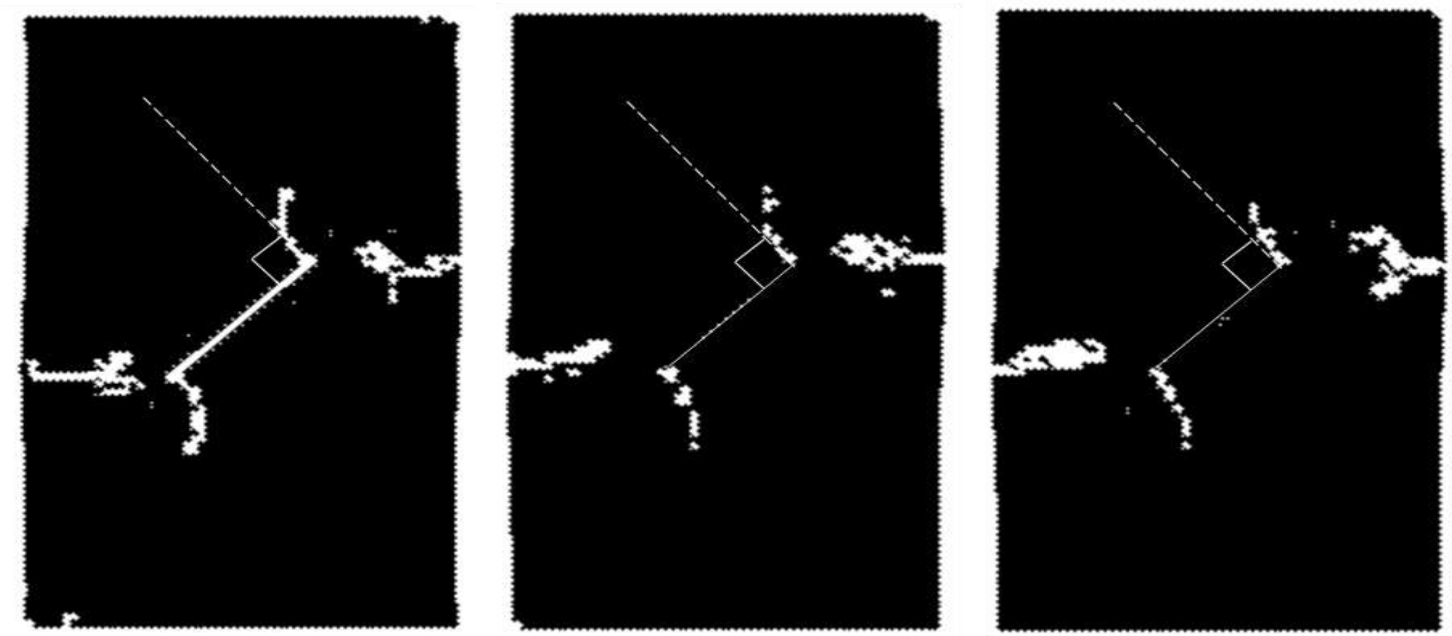

(a) sample 1 (b) sample 2 (c) sample 3

Fig. 28. Crack initiation and propagation in samples modeled by particle damage coefficient.

- **Numerical results of samples with kinetic friction as 0, 0.2, 0.4 and 0.6. The coefficient of static friction is 0.7**

It is found from the numerical results that angles between the wing cracks and the pre-existing flaws increases with increasing kinetic friction.

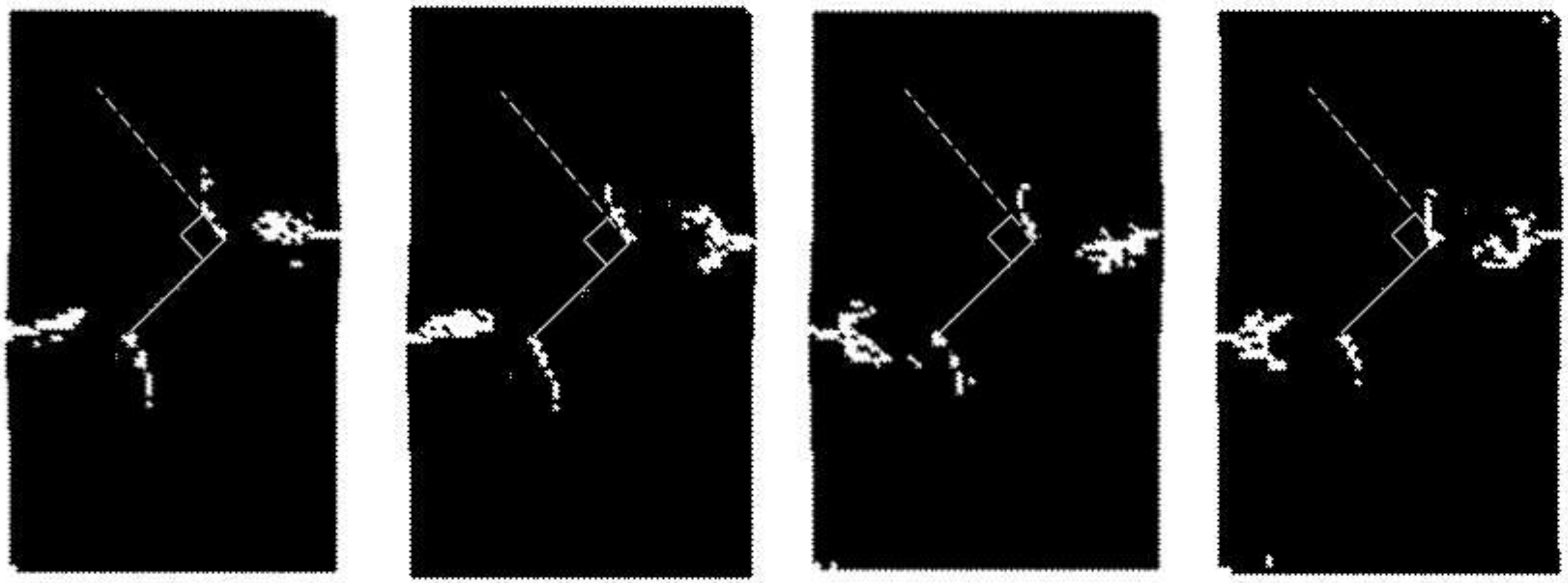

(a) sample 1 (b) sample 2 (c) sample 3 (d) sample 4

Fig. 29. Angles between the wing cracks and the pre-existing flaws.

Friction effect on the fracture process of rocks

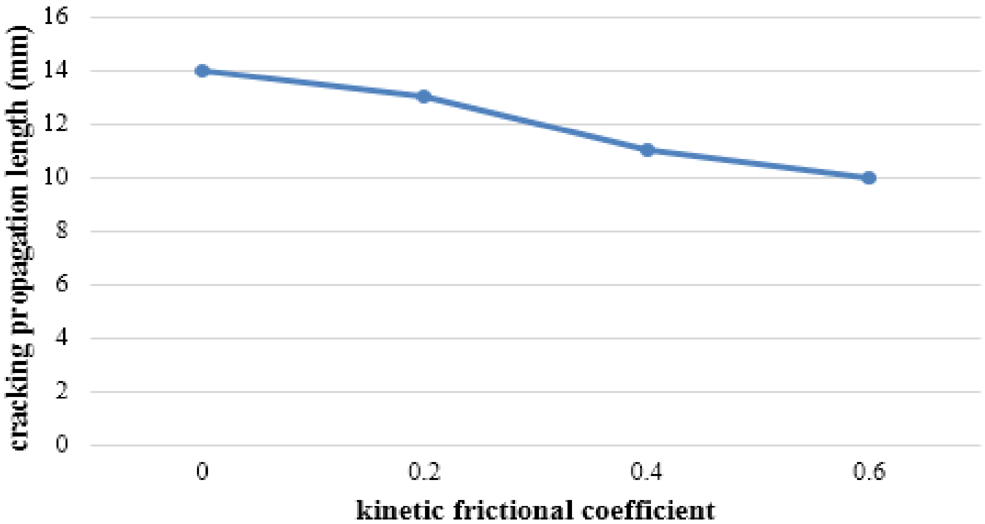

The crack growth length increases with decreasing the kinetic frictional coefficient

Fig. 30. The dependence of crack propagation length on the kinetic frictional coefficient

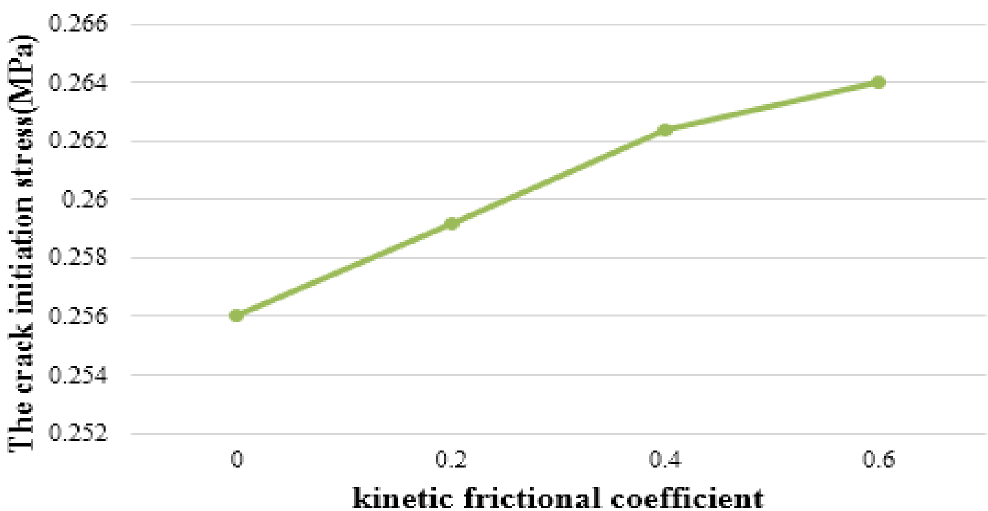

The crack initiation stress increases with increasing the kinetic frictional coefficient

Fig. 31. The dependence of crack initiation stress on the kinetic frictional coefficient

Friction effect on the fracture process of rocks

- **The initiation and propagation of cracks considering the frictional effects in the sample containing two closed flaws under uniaxial compression**

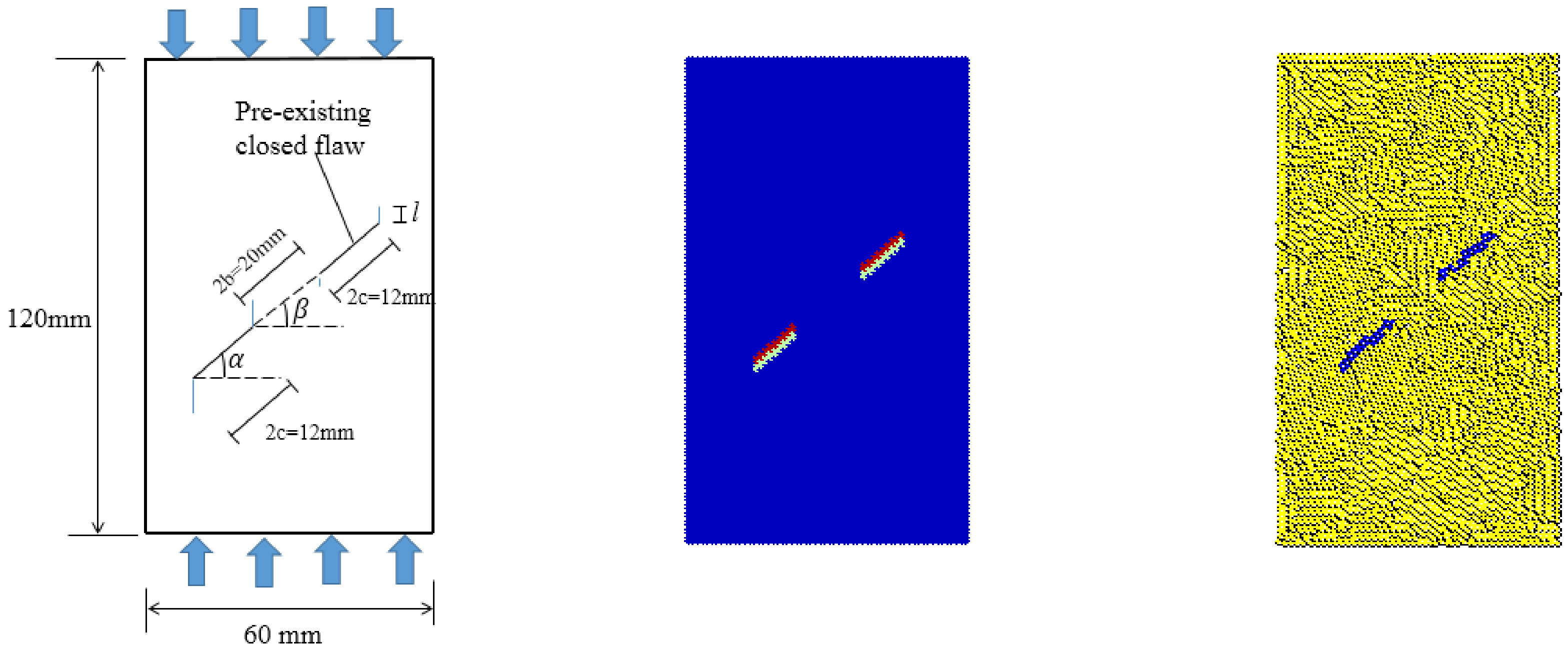

(a) The sample containing two closed flaws

(b) The numerical model of two closed flaws in GPD

(c) The numerical model of two closed flaws in PFC^{2d}

Fig. 32. Schematic of the sample containing two pre-existing flaws.

- **Numerical results of samples with static friction as 0.6, 0.7 and 0.9. The coefficient of kinetic friction is 0.6**

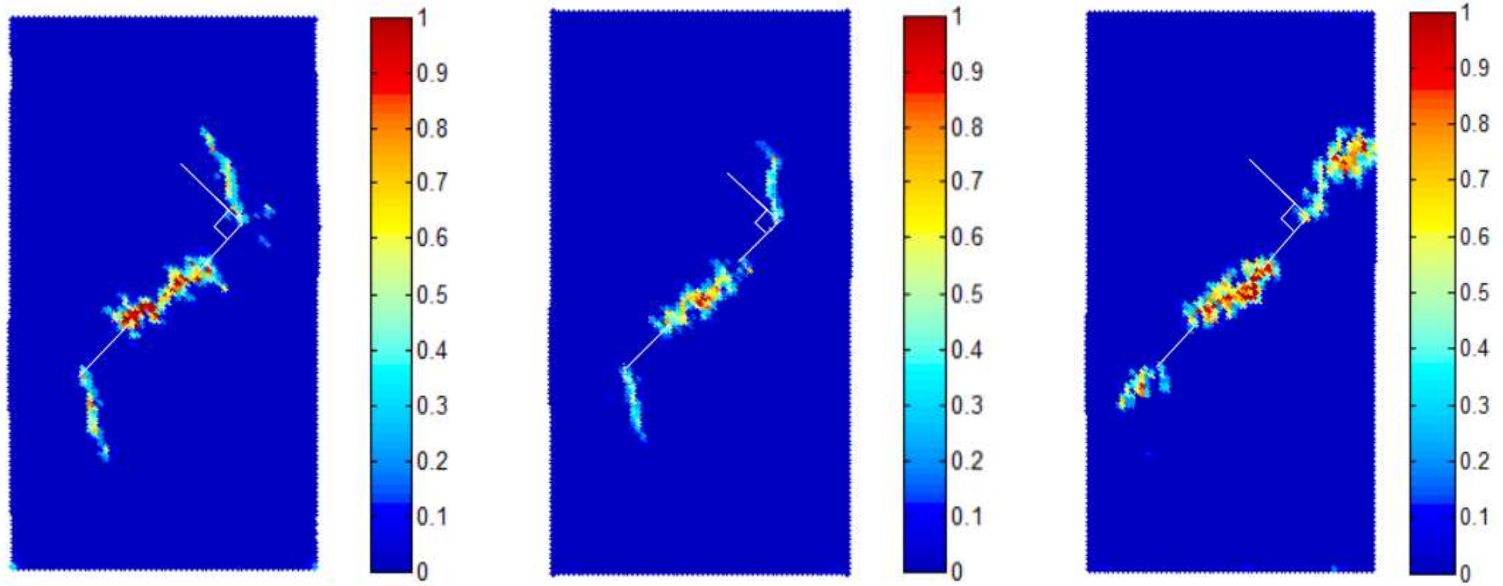

(a) sample 1(0.6) (b)sample 2(0.7) (c) sample 3(0.9)

Initiation angle of wing cracks increases with increasing static friction

Fig. 33. Initiation and propagation and coalescence of cracks in samples modeled using GPD.

Friction effect on the fracture process of rocks

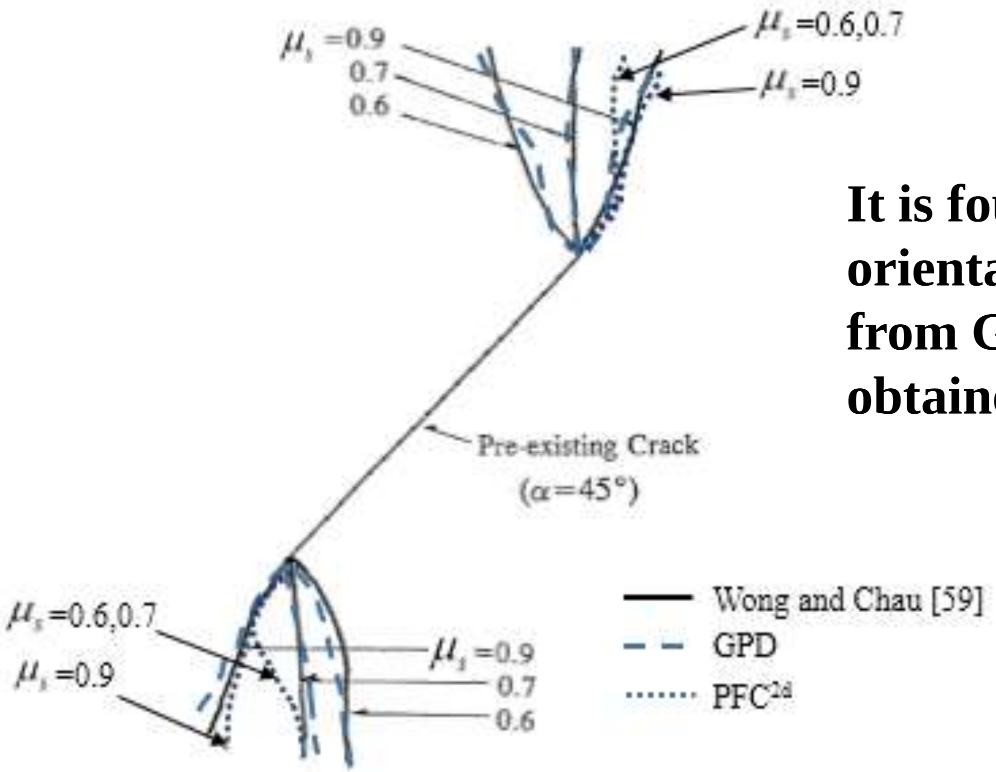

It is found from Fig.34 that the relative orientation of wing cracks obtained from GPD is in agreement with that obtained from PFC and experiments

Fig.34. The relative orientation of wing cracks versus the static frictional coefficient with respect to pre-existing flaws surfaces together with the experiment

Friction effect on the fracture process of rocks

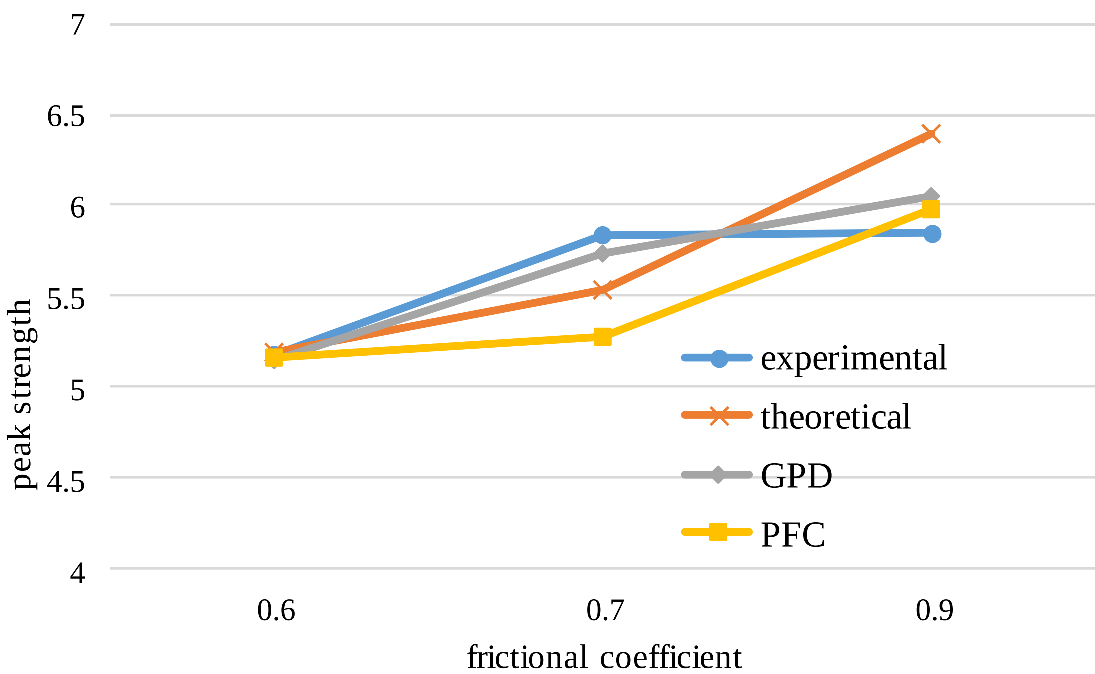

It is found from Fig.35 that peak strength obtained from GPD is in agreement with that obtained from PFC and experiments

Fig.35. The experimental (static frictional coefficent), theoretical (static frictional coefficent), GPD (static and kinetic frictional coefficents) and PFC^{2d} results (static frictional coefficent) of the peak strength of the cracked specimens.

Outline

- *Brief Description of General Particle Dynamics*
- *Growth and Coalescence of Flaws Subjected to Static Compression*
- *Kinetic Effect on Friction in the Fracture Process of Rocks*
- *Fracture in Rock-Like Materials Subjected to Impact Loads*
- *Discussions and Conclusions*

Geometries of the three-point bend

The impact machine is capable of dropping a 345 kg mass hammer with uniform initial velocity of 20 m/s is allowed to fall on a simply supported beam. The notch is just under the impact zone.

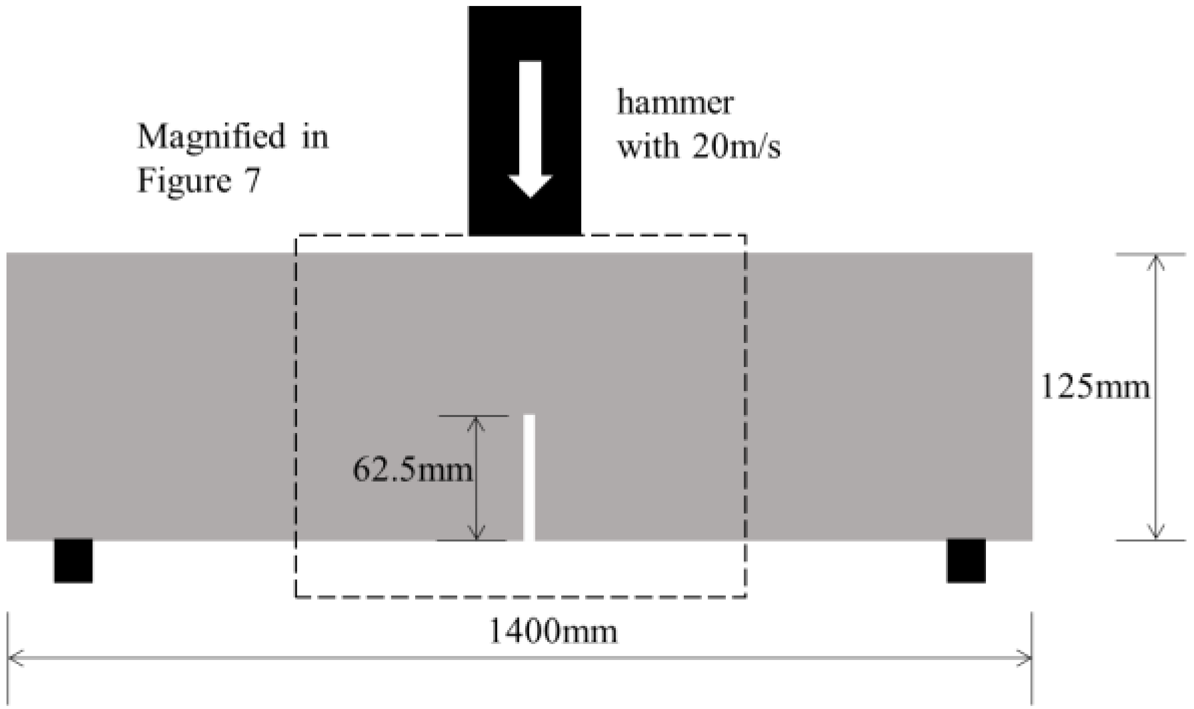

Fig.36. Initial crack location to capture crack propagation

Numerical results of the three-point bend

The crack propagation described by particle damage coefficient at different instants is depicted in Fig. 37.

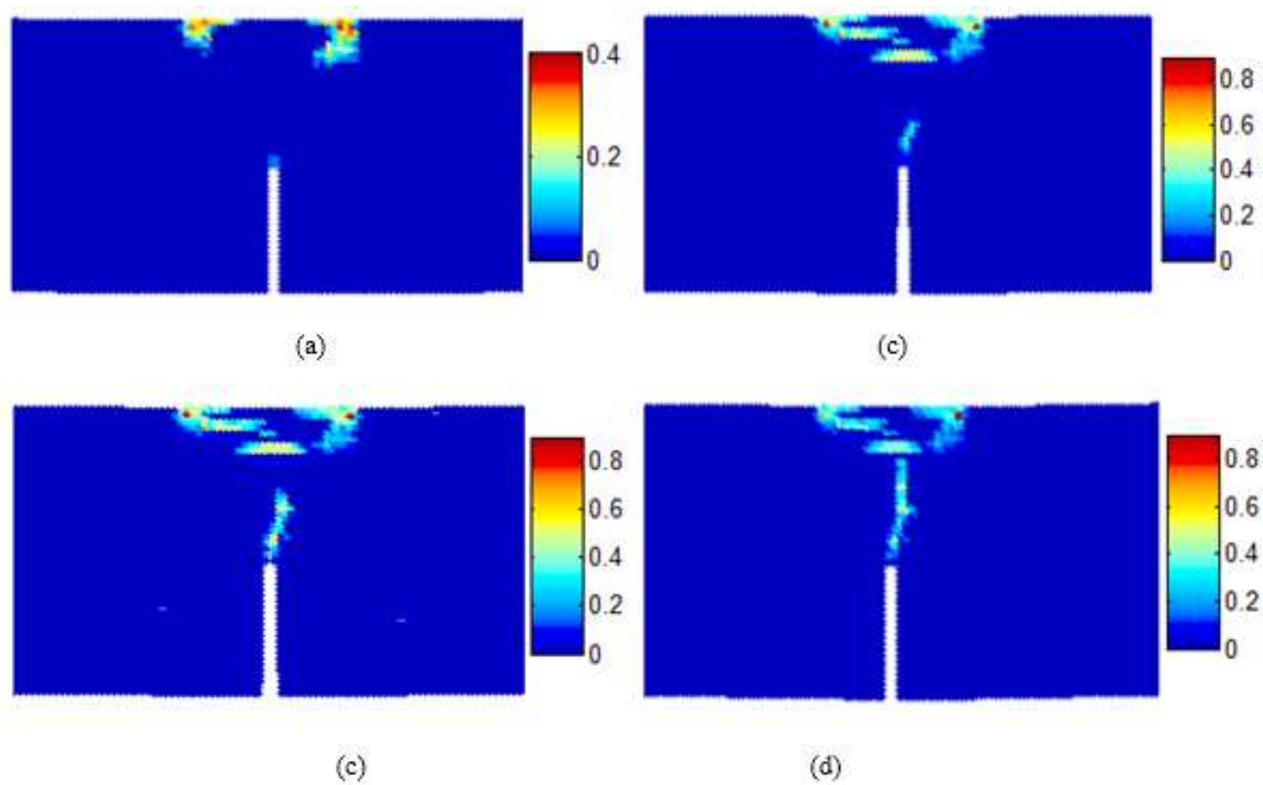

Fig.37. Tensile crack propagation described by particle damage coefficient at different times (a) 50μs (b) 100μs (c) 112.5μs (d) 125μs

Geometries of the three-point bend

In this sample, the notch is away from the impact zone and the geometric scheme is plotted in Fig. 38.

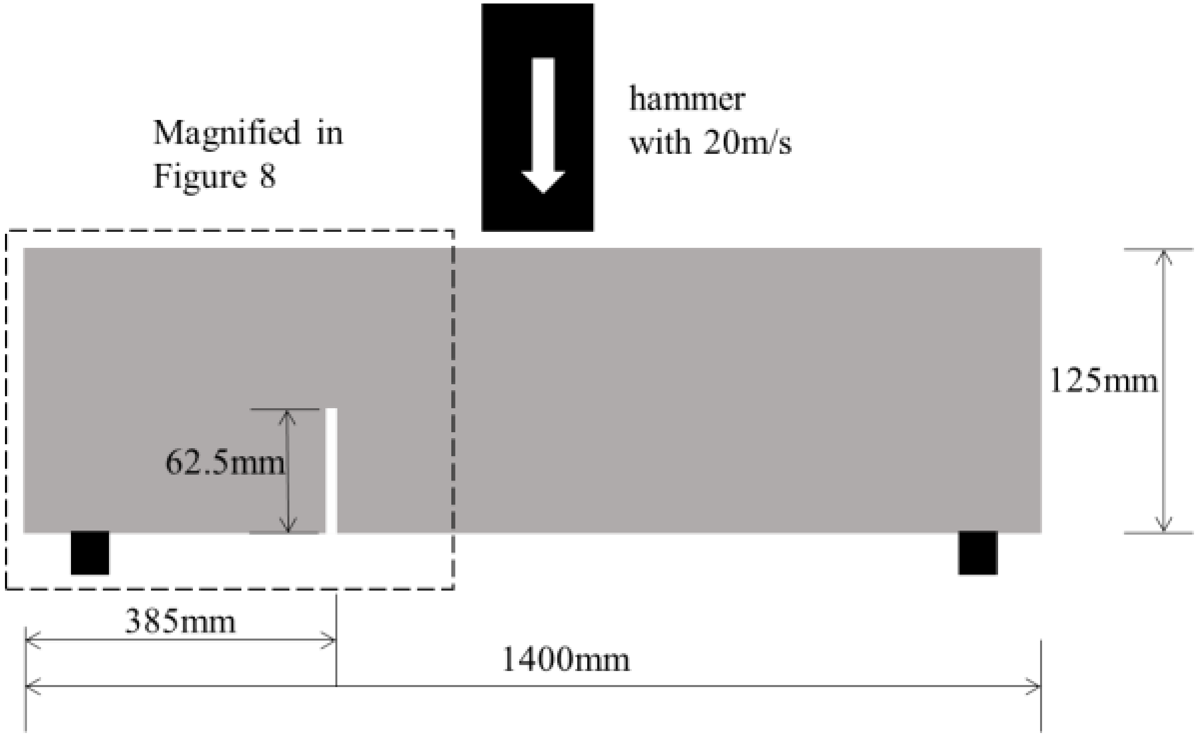

Fig.38. Initial notch location to capture shear mode propagation

Numerical results of the three-point bend

The crack growths described by particle damage coefficient at different times are plotted in Fig. 40.

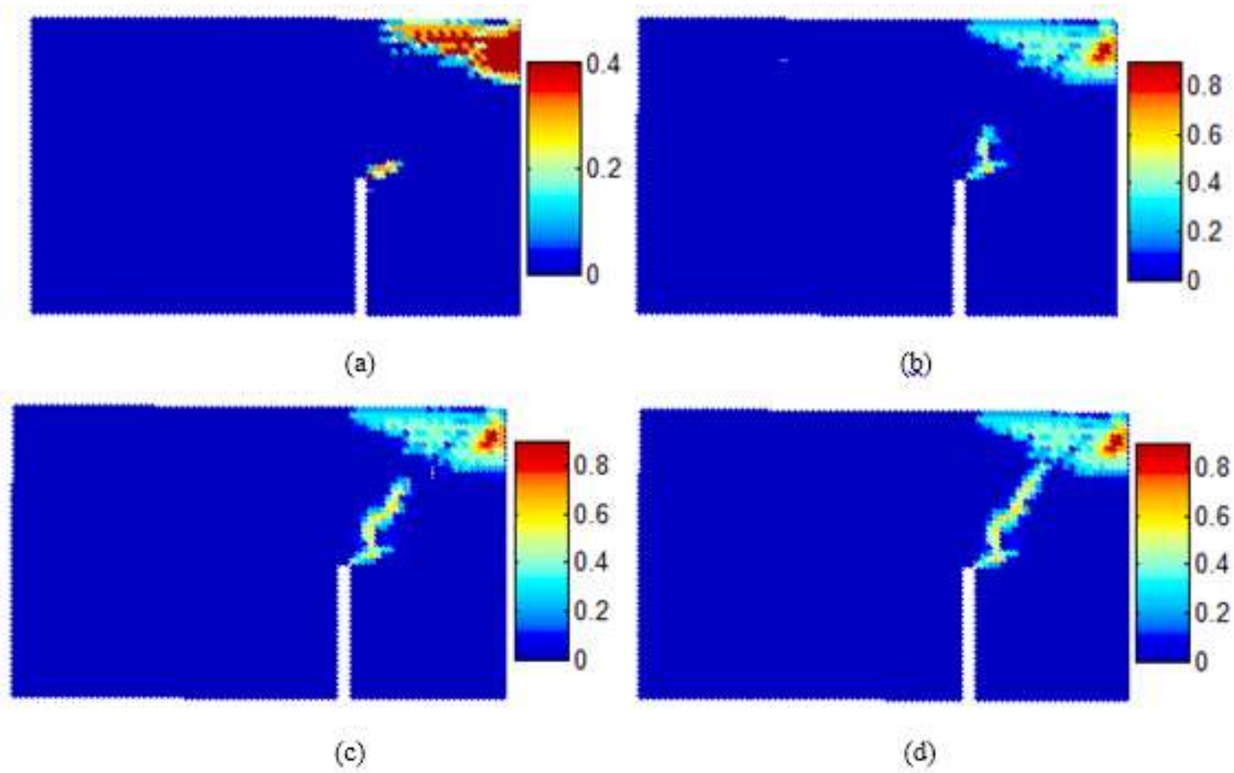

Fig.40. Shear crack propagation described by particle damage coefficient at different times (a) 50μs (b) 100μs (c) 112.5μs (d) 125μs

Geometries of the notched semi-circular granite bend

We use GPD to simulate the failure pattern of the notched semi-circular granite bend with a nominal diameter of 40 mm.

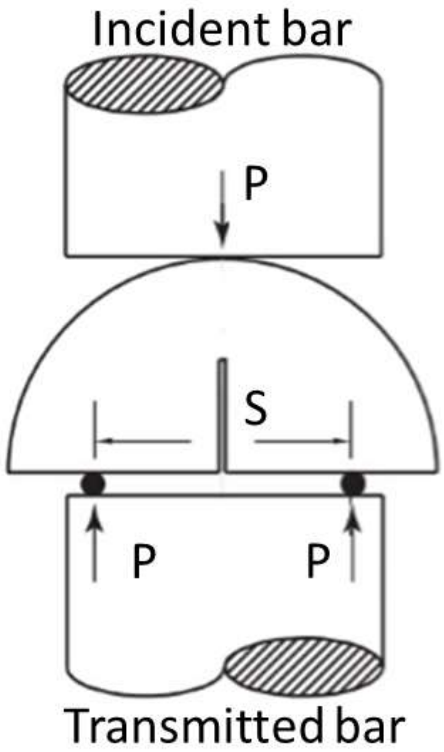

Fig.41. Schematic of the notched semi-circular bend fracture test

Numerical results of the notched semi-circular granite bend

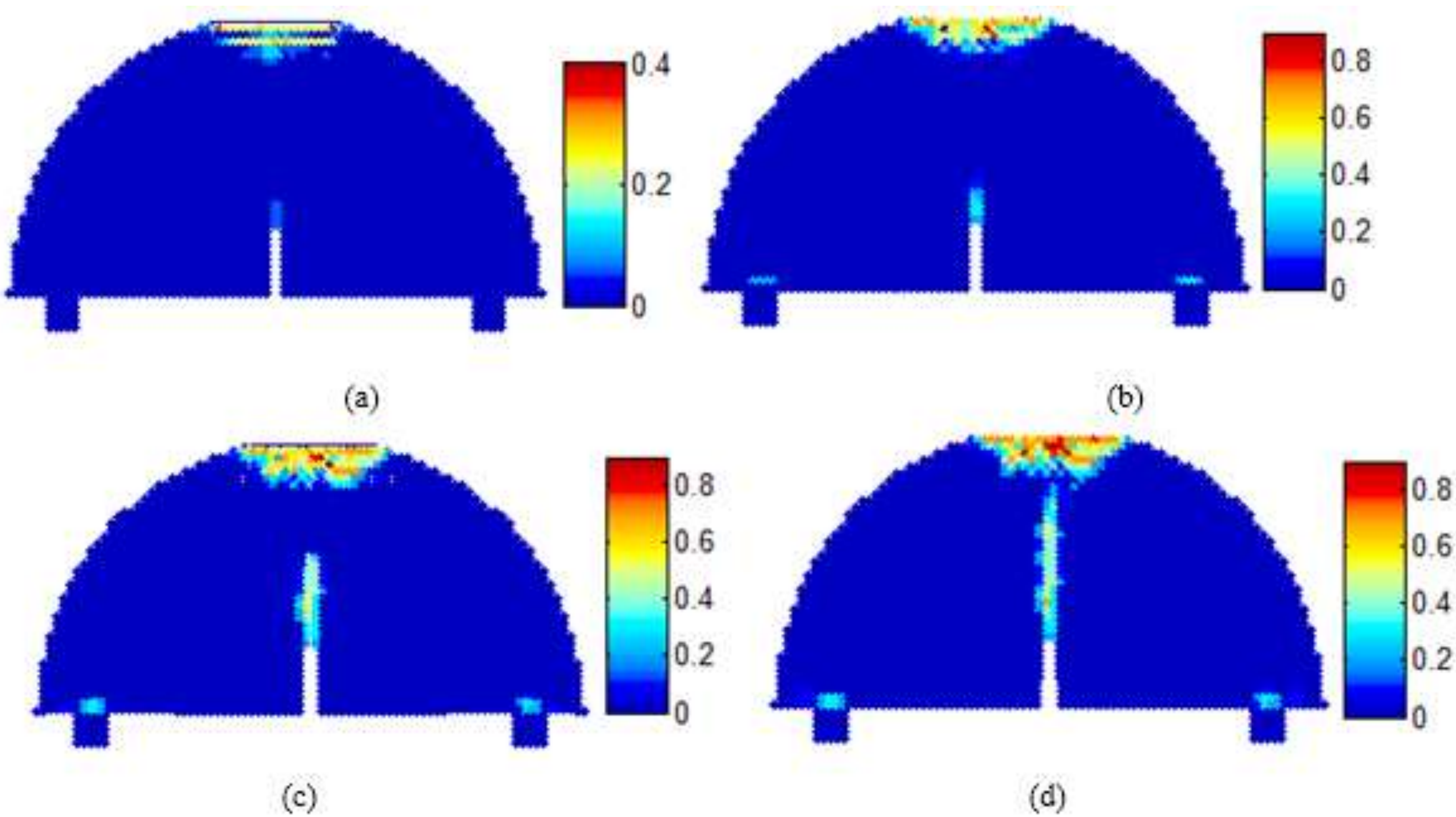

Fig.42. Tensile crack propagation described by particle damage coefficient at different times (a) 50μs (b) 100μs (c) 125μs (d) 200μs

Numerical and experimental results of the notched semi-circular granite bend

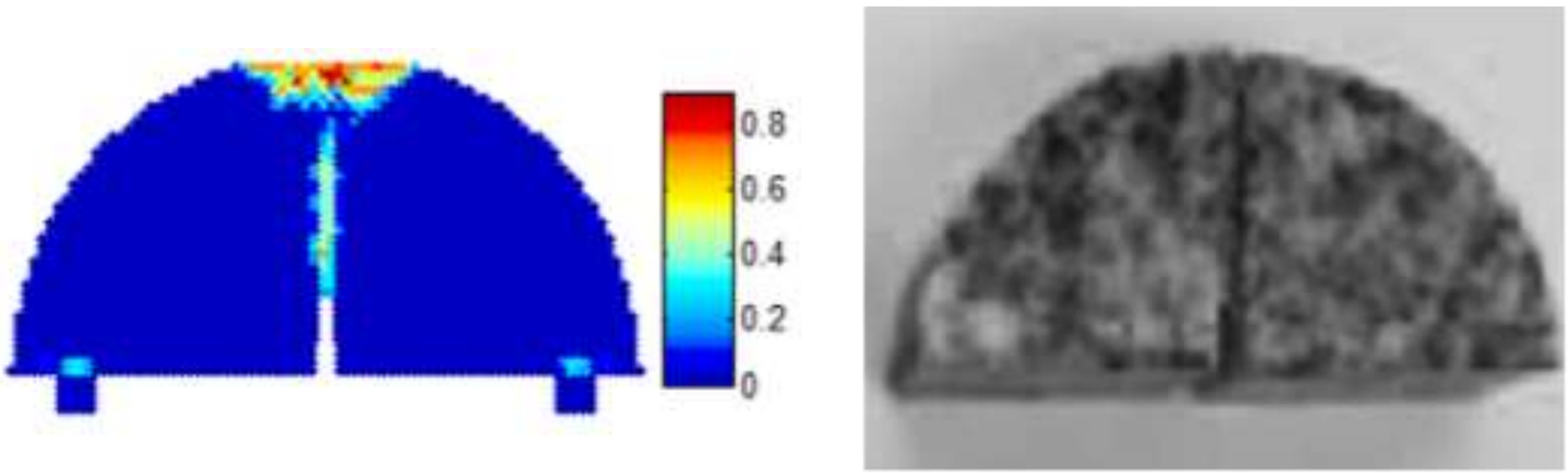

(a) (b)

Fig.43. The final crack pattern of the notched semi-circular bend (a) The final crack pattern of the notched semi-circular in numerical simulation; (b) The final crack pattern of the notched semi-circular in experiment

Geometries of the rock sample containing four pre-existing penetrating flaws

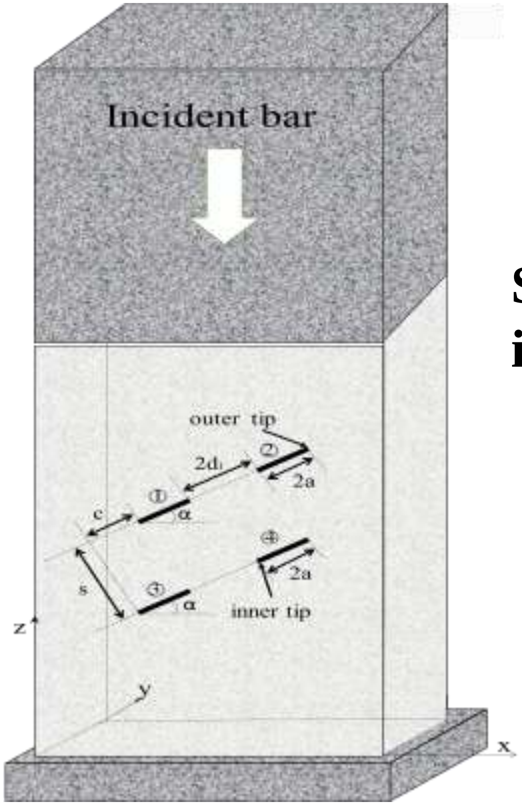

Simulation is performed with impact velocity of 2 m/s.

Fig.44. Schematic of the sample with four pre-existing flaws

Numerical results of the rock sample containing four pre-existing flaws subjected to impact loads

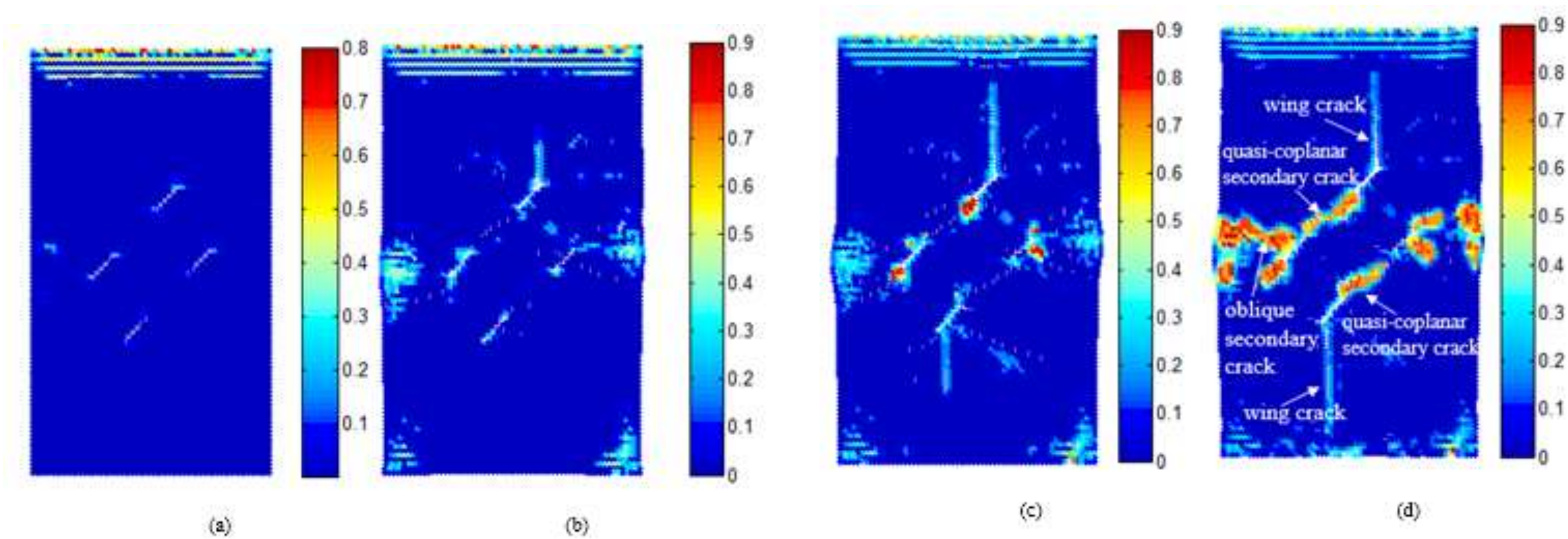

Fig.45. Crack initiation and propagation in the sample described by particle damage coefficient at different times (a) 500μs (b) 1000μs (c) 1500μs (d) 2000μs

- **Numerical results of the rock sample containing four pre-existing flaws subjected to impact loads compared with that subjected to static uniaxial compressive loads**

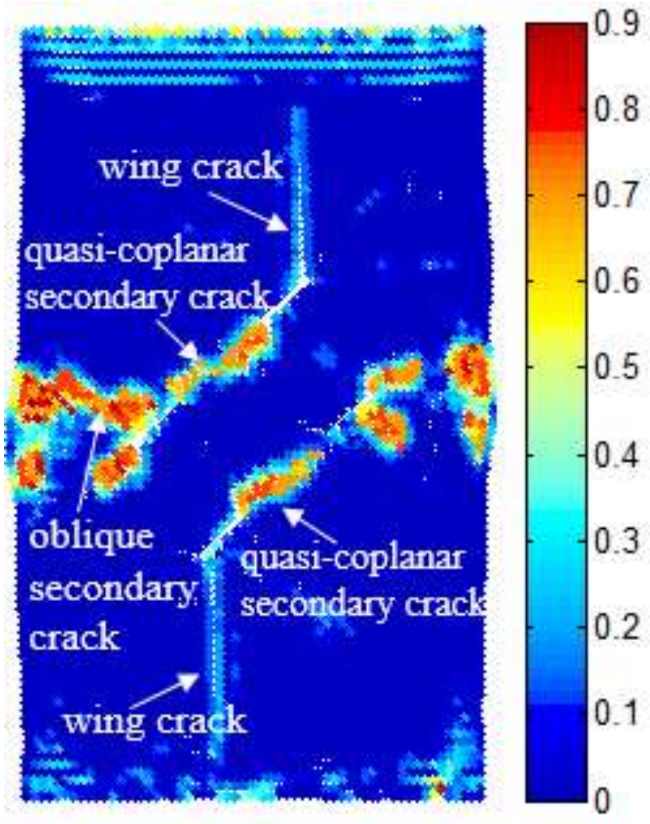

Fig.46. The final failure pattern of the sample under impact loads

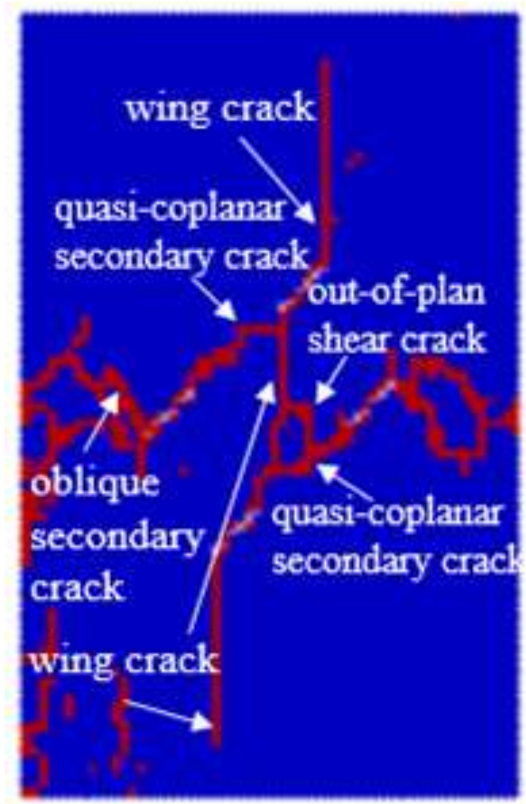

Fig.47. The final failure pattern of the sample under static uniaxial compressive loads

Outline

- *Brief Description of General Particle Dynamics*
- *Growth and Coalescence of Flaws Subjected to Static Compression*
- *Kinetic Friction in the Fracture Process of Rocks*
- *Fracture in Rock-Like Materials Subjected to Impact Loads*
- *Discussions and Conclusions*

Discussions and Conclusions

- **GPD3D is proposed to simulate propagation and coalescence processes of flaws and macro-failure of rock –like materials**

- **Tensile coalescence, pure shear, mixed mode in tensile and shear, and compression coalescence, are found and are extremely sensitive to the non-overlapping length of flaws.**

- **The initiation, propagation and coalescence processes of the wing cracks, the anti-wing cracks, the oblique secondary cracks, the out-of-plane shear cracks and the quasi-coplanar shear crack that are subjected to uniaxial and biaxial compression can be numerically simulated by GPD3D.**

- **The damaged virtual bonds are considered as the initiation of cracks. The growth path of cracks is captured through the sequence of the damaged virtual bonds. The numerical results are in good agreement with the experimental ones.**

Thanks for

your attention